

Automatic Relation-aware Graph Network Proliferation

Shaofei Cai^{1,2}, Liang Li^{1*}, Xinzhe Han^{1,2}, Jiebo Luo³, Zheng-Jun Zha⁴, Qingming Huang^{1,2,5}

¹Key Lab of Intell. Info. Process., Inst. of Comput. Tech., CAS, Beijing, China

²University of Chinese Academy of Sciences, Beijing, China, ³University of Rochester

⁴University of Science and Technology of China, China, ⁵Peng Cheng Laboratory, Shenzhen, China

{shaofei.cai, xinzhe.han}@vip1.ict.ac.cn, liang.li@ict.ac.cn,
jluo@cs.rochester.edu, zhazj@ustc.edu.cn, qmhuang@ucas.ac.cn

Abstract

Graph neural architecture search has sparked much attention as Graph Neural Networks (GNNs) have shown powerful reasoning capability in many relational tasks. However, the currently used graph search space overemphasizes learning node features and neglects mining hierarchical relational information. Moreover, due to diverse mechanisms in the message passing, the graph search space is much larger than that of CNNs. This hinders the straightforward application of classical search strategies for exploring complicated graph search space. We propose Automatic Relation-aware Graph Network Proliferation (ARGNP) for efficiently searching GNNs with a relation-guided message passing mechanism. Specifically, we first devise a novel dual relation-aware graph search space that comprises both node and relation learning operations. These operations can extract hierarchical node/relational information and provide anisotropic guidance for message passing on a graph. Second, analogous to cell proliferation, we design a network proliferation search paradigm to progressively determine the GNN architectures by iteratively performing network division and differentiation. The experiments on six datasets for four graph learning tasks demonstrate that GNNs produced by our method are superior to the current state-of-the-art hand-crafted and search-based GNNs. Codes are available at <https://github.com/phython96/ARGNP>.

1. Introduction

Graph neural networks (GNNs), as a dominant paradigm to handle graph-structured data, have significantly promoted the performance in many relation reasoning tasks, such as molecular prediction [8, 16, 19, 25], social network analysis [36, 41], 3D point cloud recognition [31, 32, 48, 55],

object detection [20, 23], semantic segmentation [24, 34, 54], few-shot learning [27, 51, 61], etc. Despite their great success, the architectures of GNNs are usually manually designed, which requires tremendous expert knowledge and intensive trial and error. To explore advanced GNN architectures and reduce the human intervention, researchers attempt to automate the design process with the help of neural architecture search (NAS) [18, 37, 44, 65, 66] and have achieved superior performance. This is known as graph neural architecture search, where there are two most critical components: (1) graph search space and (2) search strategy.

The graph search space defines which graph neural networks can be represented in principle, determining the upper bound of networks' reasoning capability. Current graph search space mainly focuses on designing node-learning operations, which is categorized into macro search space [33, 44] and micro search space [12, 18, 37, 66]. The former explores the combinations of existing message passing mechanisms (*i.e.*, using general-purpose GNNs as candidate operations), while the latter emphasizes the construction for novel ones (*i.e.*, designing fine-grained operations such as node aggregating and feature combining functions). However, they all neglect mining the latent hierarchical relational information associated with edges. In fact, relational information can provide anisotropic guidance for message aggregation of neighboring nodes, which is critical for constructing relation-guided message passing mechanisms. Motivated by this, in this paper, we explore designing micro graph search space from the perspective of learning both hierarchical relation and node features.

The search strategy details how to explore search space, determining the search efficiency and effect. Some early works [18, 65, 66] apply reinforcement learning (RL) based strategy to search for GNNs by building, training, and evaluating various graph neural architectures from scratch, which is extremely time-consuming. Recently, due to the high computational efficiency, one-shot differentiable strategies [12, 33, 37] have attracted a lot of interest, which

*Corresponding author.

consists of three stages: supernet training, subnet searching, and subnet retraining. They boost the search efficiency from the parameter sharing among subnets and supernet. Using the auxiliary supernet can avoid training each child graph neural architecture individually, but this may cause severe subnet interference [63, 64]. Besides, it is limited in searching large GNN architectures due to the quadratic complexity of storing and training the supernet. As a compromise, researchers introduce the cell trick where the architecture is a stack of several same building blocks [12, 33, 37, 40]. This shifts the searching objective from the whole architecture to small cells but seriously narrows the original search space. The above limitations, *i.e.* the subnet interference, the high space-time complexity and the shrink of search space, bring a severe negative impact for graph neural architecture search.

In this paper, we propose the Automatic Relation-aware Graph Network Proliferation (ARGNP) to efficiently search the optimal GNN architectures with a relation-guided message passing mechanism. First, we design a dual relation-aware graph search space comprising both relation and node search space, as shown in Figure 2. The relation search space introduces diverse relation-mining operations to extract relational information hidden in edge-connected nodes. It allows arbitrary valid connection modes among relation-mining operations and forms the hierarchical relation-learning structure. Different connection modes result in the group of relation features with different message-passing preferences, which favors different graph tasks. The node search space defines a series of node-learning operations which implements the anisotropic message aggregation under the guidance of relation features.

Second, analogous to cell proliferation, we devise a novel search paradigm called *network proliferation* to progressively explore the graph search space. Instead of directly optimizing the global supernet, we search the final graph neural architecture by iteratively performing network division and network differentiation. Figure 1 shows one iteration process. During network division, each intermediate feature vertex is divided into two parts. One retains original operations and connections while the other builds a local supernet. Network differentiation aims to differentiate the local supernet into a specific subnet. Theoretically, we proved that such a search paradigm achieves the linear space-time complexity. This enables our search to thoroughly free from the cell trick. The network proliferation decomposes the training of global supernet into sequential local supernets optimization, which alleviates the interference among child graph neural architectures.

Our contributions are summarized as follows: (1) A novel dual relation-aware graph search space comprising both node and relation search space. It can derive GNNs with a relation-guided message passing mechanism. (2) A

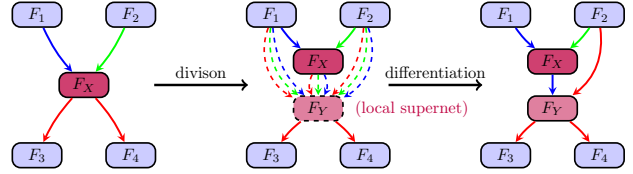


Figure 1. **One iteration of the proposed network proliferation search paradigm.** $F_{(\cdot)}$ denotes the intermediate feature vertex in an architecture. The edges with different colors are associated with different operations. F_Y is the newly divided part of F_X , which joins F_1 , F_2 and F_X to build a local supernet.

network proliferation search paradigm. It sequentially performs network division and differentiation to explore the optimal GNN architecture within linear space-time complexity. (3) Experiment results on six datasets for four classical graph learning tasks show that our method outperforms human-crafted and other search-based GNNs by a large margin. The code will be released publicly.

2. Related Work

Graph Neural Networks (GNNs) have been successfully applied to operate on the graph-structure data [9, 10, 15, 21, 29, 53, 59, 62]. Current GNNs are constructed on message passing mechanisms and can be categorized into two groups, isotropic and anisotropic. Isotropic GNNs [21, 29, 59] aim at extending the original convolution operation to graphs. Anisotropic GNNs enhance the original models with anisotropic operations on graphs [45], such as gating and attention mechanism [9, 42, 43, 53, 62]. Anisotropic methods usually achieve better performance, since they can weigh the importance of edges according to the node features and implement the adaptive feature aggregation.

Neural Architecture Search (NAS) aims at automatically finding the optimal neural architectures specific to dataset [4, 11, 14, 32, 38, 40, 40, 46, 57, 67]. Search space and strategy are the most essential components in NAS. Search space defines which architectures can be represented in principle. Search strategy details how to explore the search space. Methods can be mainly categorized into three groups, *i.e.*, reinforcement learning (RL) [4, 46, 67], evolutionary algorithms (EA) [39, 49, 50] and gradient-based (GB) [11, 14, 32, 38, 40, 60]. Benefiting from the high efficiency, gradient-based differentiable search strategies attracted the attention of increasing researchers.

Graph Neural Architecture Search (GNAS) is proposed to automatically find the best GNNs for the given specific graph task. The current GNAS methods [12, 18, 37, 44, 65, 66] mainly focus on designing graph search space by introducing neighbor aggregation, activation functions, *etc.*, but neglect the importance of relation mining. To our best knowledge, we are the first to take mining relational information into account during devising graph search space.

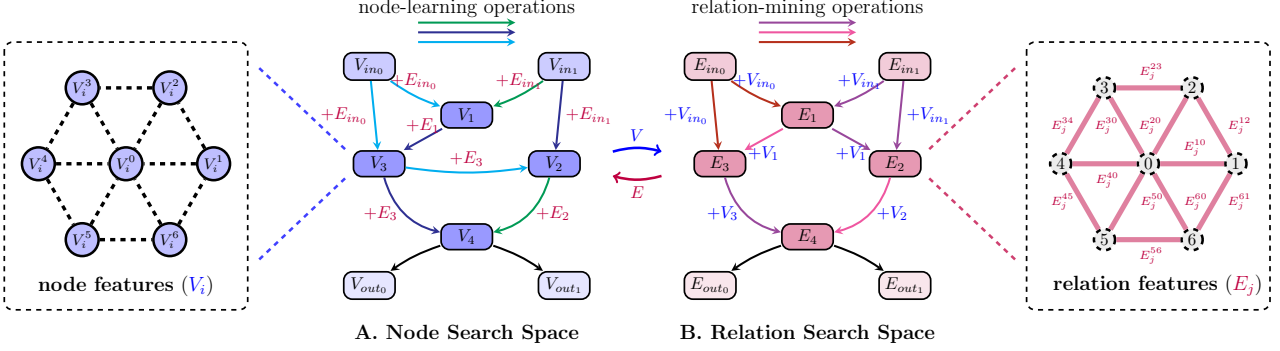


Figure 2. **Our dual relation-aware graph search space.** It comprises node and relation search space. The vertex V_i and vertex E_j denote a group of node and relation features on the graph, respectively. $+E_j$ means that learning node features require the guidance of relation features. $+V_i$ means that the node features are required when extracting relational information.

3. Method

3.1. Preliminaries

A graph neural architecture uses graph-structured data as input and outputs high-dimensional node and edge features (relation features). The input data can be represented as $\{G, V_{in}, E_{in}\}$, where G is the input graph structure with n nodes and m edges, $V_{in} \in \mathbb{R}^{n \times d_V}$ denotes the input node features, $E_{in} \in \mathbb{R}^{m \times d_E}$ denotes the input edge features, d_V and d_E denote the feature dimension. Notably, if there is no original edge feature in the dataset, we initialize E_{in} with $[1, \dots, 1] \in \mathbb{R}^{m \times 1}$ for subsequent relation learning. Our dual relation-aware graph search space comprises both node and edge search space. The derived computation structure of node or relation search space is a directed acyclic graph (DAG). To avoid confusion, the node and edge in the DAG is renamed to “vertex” and “link”, where “vertex” denotes an intermediate features (V_i or E_j), the “link” is associated with an operation \mathcal{O} or a mixture operation $\bar{\mathcal{O}}$.

3.2. Relation-aware Graph Search Space

In this subsection, we detail how our dual relation-aware graph search space is devised. As shown in Figure 2, it comprises node search space and relation search space. These two spaces are not individual in essence, instead, they communicate information with each other. The relational information is extracted from node features. In turn, it provides anisotropic guidance for learning better node features.

Node search space. The computation structure derived by node search space is a directed acyclic graph, which consists of an ordered sequence of $N+4$ vertices, which constitutes the set $\{V_{in_0}, V_{in_1}, V_1, \dots, V_N, V_{out_0}, V_{out_1}\}$. Each vertex is a latent representation denoted as V_i (i.e., node features in a GNN layer, as shown in the left of Figure 2), where i is its topological order in the DAG. In order to be compatible with the cell trick, we introduce two input vertices and two output vertices. V_{in_0} and V_{in_1} are the outputs of previous two cells while V_{out_0} and V_{out_1}

are the inputs of post two cells. In fact, our method can thoroughly free from the cell trick. In this situation, we have $V_{in_0} = V_{in_1}$, $V_{out_0} = V_{out_1}$. Each directed link (i, j) in the DAG is associated with one node-learning operation $\mathcal{O}_V^{(i,j)}$, that transforms the information from V_i to V_j , guided by relation features E_i . The transformed information is denoted as $V_{i \rightarrow j} = \mathcal{O}_V^{(i,j)}(V_i, E_i, f_{i,j})$, where $f_{i,j}$ is an aggregating function which takes multiset as input, such as *mean*, *max*, *sum*, *std*, etc. We leverage feature-wise linear modulation (FiLM) mechanism [10] to implement the anisotropic guidance of message propagation. This allows the model to dynamically up-weight and down-weight node features based on the relational information. Specifically, we compute an element-wise affine transformation γ and β based on the input relation features E_i and use it to modulate the incoming messages during message passing. Given a node t on the graph, its transformed feature $V_{i \rightarrow j}^t$ is formulated as follows

$$V_{i \rightarrow j}^t = f_{i,j}(\{\gamma_{s,t} \odot V_i^s + \beta_{s,t} | s \in \mathcal{N}(t)\}), \quad (1)$$

$$\gamma_{s,t}, \beta_{s,t} = g(E_i^{s,t}; \theta),$$

where $g(\cdot)$ is a two-layer multilayer perceptron to compute affine transformation with the learnable parameters θ , $\mathcal{N}(t)$ denotes the set of neighbors of target node t on the graph. Following previous works [12, 33, 37, 40], we allow two inputs for each intermediate vertex, i.e., $V_i = V_{p_1 \rightarrow i} + V_{p_2 \rightarrow i}$, where $p_1, p_2 \in \{in_0, in_1, 1, 2, \dots, i-1\}$. For each node-learning operation, its aggregating function is optional. Different aggregating function $f_{i,j}$ captures different types of information. For example, *sum* captures the structural information [59], *max* captures the representative information, *mean* and *std* captures the statistical information from the neighboring nodes. The node search space has 8 candidate node-learning operations: *V_MAX*, *V_SUM*, *V_MEAN*, *V_STD*, *V_GEM2*, *V_GEM3*, *skip-connect*, and *zero* operation. We detail all eight node-learning operation options in the supplementary material.

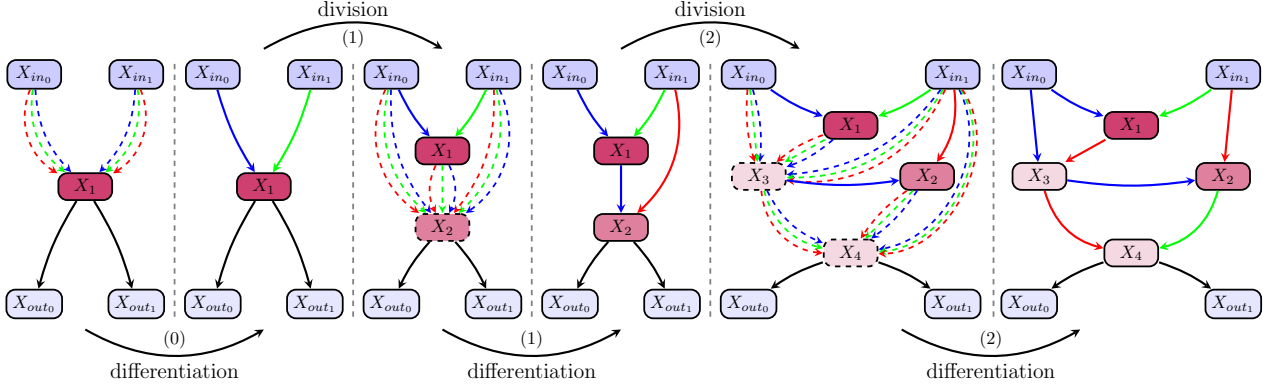


Figure 3. **Illustration of network proliferation search paradigm.** It comprises two procedures of network division and differentiation. The edges with different colors are associated with different operations. A group of dashed edges denotes a mixture operation. A local supernet comprises of three mixture operations pointing to one feature vertex. (i) denotes the i -th iteration.

Relation search space. The computation structure derived by relation search space is also a directed acyclic graph with the same number of vertices. Each vertex E_i is a latent relation representation (*i.e.*, edge features in a GNN layer, as shown in the right of Figure 2). The directed link (i, j) in the DAG is associated with a relation-mining operation $o_{\mathcal{E}}^{(i,j)}$. It extracts relational information from node features V_i . The extracted information is joined with E_i to obtain higher order relation representation $E_{i \rightarrow j} = o_{\mathcal{E}}^{(i,j)}(V_i, E_i, h_{i,j})$. $h_{i,j}$ is a relation-mining function, such as *subtraction*, *hardmard product*, *gauss kernel*, *etc.* Given a specific edge (s, t) on the graph, $E_{i \rightarrow j}^{s,t}$ can be computed using feature-wise linear modulation (FiLM):

$$\begin{aligned} E_{i \rightarrow j}^{s,t} &= \gamma_{s,t} \odot E_i^{s,t} + \beta_{s,t}, \\ \gamma_{s,t}, \beta_{s,t} &= h_{i,j}(V_i^s, V_i^t; \theta), \end{aligned} \quad (2)$$

where $\gamma_{s,t}, \beta_{s,t}$ is the affine transformation learned by $h_{i,j}$, θ is the learnable parameters. This allows adaptive relational information fusion. Similar to node search space, we assume that each intermediate vertex has and only has two inputs, *i.e.*, $E_i = E_{p_1 \rightarrow i} + E_{p_2 \rightarrow i}$, where $p_1, p_2 \in \{in_0, in_1, 1, 2, \dots, i-1\}$. Different relation-mining operations focus on extracting different types of relational information. For example, *subtraction* captures the relative change while *hardmard product* emphasizes on the commonalities between the edge-connected nodes. The relation search space has 8 candidate relation-mining operations: *E_SUB*, *E_GAUSS*, *E_HAD*, *E_MAX*, *E_SUM*, *E_MEAN*, *skip-connect*, and *zero* operation. Eight candidate options of the relation-mining function are detailed in the supplementary material.

3.3. Network Proliferation Search Paradigm

We detail how the proposed network proliferation search paradigm explores a single search space (*e.g.*, node or rela-

Algorithm 1 Network Proliferation Search Paradigm

Input: a search algorithm \mathcal{A} , architecture size \mathcal{S}
Output: a graph neural architecture defined by $\{\mathbb{V}, \mathbb{L}\}$
Define: $e(X_s, X_t, O)$ is a link from X_s to X_t with an operation O , where $O \in \{o, \bar{o}\}$, \bar{o} is the mixture operation

- 1: $\mathbb{V} \leftarrow \{X_1\}$
- 2: $\mathbb{L} \leftarrow \{e(X_{in_0}, X_1, \bar{o}), e(X_{in_1}, X_1, \bar{o})\}$
- 3: **while** True **do**
- 4: **// network differentiation**
- 5: $\mathbb{V}_r \leftarrow \mathbb{V} \cup \{X_{in_0}, X_{in_1}\}$
- 6: Create a graph neural architecture \mathcal{G} from $\{\mathbb{V}_r, \mathbb{L}\}$
- 7: Initialize \mathcal{G} with new parameters
- 8: Perform search algorithm: $\mathbb{L} \leftarrow \mathcal{A}(\mathcal{G})$
- 9: **if** $len(\mathbb{V}) \geq \mathcal{S}$ **then**
- 10: **return** $\{\mathbb{V}_r, \mathbb{L}\}$
- 11: **// network division**
- 12: $\mathbb{V}_{tmp} \leftarrow \mathbb{V}, \mathbb{L}_{tmp} \leftarrow \mathbb{L}, l \leftarrow len(\mathbb{V})$
- 13: **for** X_i in \mathbb{V}_{tmp} **do**
- 14: $\mathbb{V} \leftarrow \mathbb{V} \cup \{X_{i+l}\}$
- 15: $\mathbb{L} \leftarrow \mathbb{L} \cup \{e(X_i, X_{i+l}, \bar{o})\}$
- 16: **for** $e(X_s, X_t, O)|_{t=i}$ in \mathbb{L}_{tmp} **do**
- 17: $\mathbb{L} \leftarrow \mathbb{L} \cup \{e(X_s, X_{i+l}, \bar{o})\}$
- 18: $\mathbb{L}_{tmp} \leftarrow \mathbb{L}$
- 19: **for** $e(X_s, X_t, O)|_{s \in \mathbb{V}_{tmp}, s+l \neq t}$ in \mathbb{L}_{tmp} **do**
- 20: $\mathbb{L} \leftarrow \mathbb{L} \cup \{e(X_{s+l}, X_t, O)\} / \{e(X_s, X_t, O)\}$

tion search space) for simplicity. Since our dual relation-aware graph search space comprising node and relation search space is symmetric, it can be generalized to search the whole dual space simultaneously.

Motivated by the observation that a well-performed small architecture can provide a good skeleton for building a larger one (shown in Figure 4), we can efficiently obtain the expected large architecture through iterative search

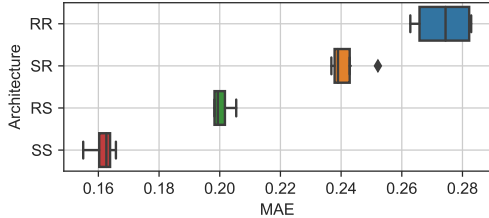


Figure 4. **Boxplots of 8-layer architectures on ZINC.** “R” and “S” denote the random and SGAS [32] search strategies, respectively. *e.g.*, architecture “RS” is constructed by sequentially performing random search, network division and SGAS search. The architecture size after the first and the second search is 4 and 8. Comparing “RR” with “SR”, “RS” with “SS”, we find that a pre-searched architecture is useful for subsequent search.

based on the current small architecture. We detail this procedure in Figure 3 and Algorithm 1. Each iterative search comprises of two subprocedures, *i.e.*, network division, and network differentiation. Network division builds a $2\times$ larger architecture based on the current architecture, where each feature vertex is divided into two parts. One part that retains original operations and connections is called parent vertex (X_p), whose role is to provide the architecture skeleton. The other one is called newly divided vertex (X_n), which joins X_p and X_p ’s two input vertices X_{p_1}, X_{p_2} to build a local supernet. We define the mixture operation is parameterized by architectural parameters $\alpha^{(i,j)}$ as a softmax mixture over all the possible operations within the operation space \mathcal{O} , *i.e.*, $\bar{o}^{(i,j)}(X_i) = \sum_{o \in \mathcal{O}} \frac{\exp(\alpha_o^{(i,j)})}{\sum_{o' \in \mathcal{O}} \exp(\alpha_{o'}^{(i,j)})} o(X_i)$. The local supernet contains three mixture operations, which is represented as follows,

$$X_n = \bar{o}^{(p,n)}(X_p) + \bar{o}^{(p_1,n)}(X_{p_1}) + \bar{o}^{(p_2,n)}(X_{p_2}). \quad (3)$$

Since the local supernet contains $C_3^2 \times |\mathcal{O}|$ candidate local subnets, we need to discretize it to one specific subnet. This is called network differentiation. During this procedure, we can adopt any search algorithms [13, 22, 33, 40, 58, 60], that can discretize the supernet to the subnet. After the network differentiation, each mixture operation in the architecture is replaced with one specific operation. The algorithm terminates until the size of the architecture reaches the pre-defined threshold.

Next, we analyze the complexity of our network proliferation search paradigm. The running time and occupied memory are proportional to the number of operations. It requires $\log(N)$ iterations for searching for architecture with N feature vertices. During the i -th iteration, there are $2^{i-1} \times 2$ operations and $2^{i-1} \times 3$ mixture operations, *i.e.*, $2^i + 3 \times 2^{i-1}|\mathcal{O}|$ operations in total. So the whole complexity is $O(\sum_{i=1}^{\log(N)} 2^i + 3 \times 2^{i-1}|\mathcal{O}|) = O(N|\mathcal{O}|)$. Compared with vanilla DARTS [40] ($O(N^2|\mathcal{O}|)$ complexity), our method reduces the complexity from quadratic to linear. This enables ours to directly search for large neu-

ral architectures without relying on the cell trick, and this also enlarges the global search space. For example, we try to search for an architecture with $N = 16, |\mathcal{O}| = 8$. In general, due to the high complexity, the DARTS stacks 4 cells with 4 feature vertices in each of them, resulting in 3.0×10^9 candidate architectures. Compared with vanilla DARTS, our search paradigm can explore up to 3.4×10^{36} candidate architectures using comparable resources.

4. Experiments

4.1. Experimental Setups

Dataset. We evaluate our method on six datasets, *i.e.*, ZINC [26], CLUSTER [17], CIFAR10 [30], TSP [17], ModelNet10 [56], ModelNet40 [56] across four different graph learning tasks (node classification, edge classification, graph classification and graph regression). ZINC is one popular real-world molecular dataset of 250K graphs, whose task is graph property regression, out of which we select 12K for efficiency following works [12, 15, 17]. CLUSTER is the node classification tasks generated via Stochastic Block Models [1], which are used to model communications in social networks by modulating the intra-community and extra-community connections. CIFAR10 is the original classical image classification dataset and converted into graphs using superpixel [2] algorithm to test graph classification task. TSP dataset is based on the classical *Travelling Salesman Problem*, which tests edge classification on 2D Euclidean graphs to identify edges belonging to the optimal TSP solution. ModelNet is a dataset for 3D object recognition with two variants, ModelNet10 and ModelNet40, which comprise objects from 10 and 40 classes, respectively. We sample 1024 points for each object as input and use k -NN algorithm to construct the edges ($k = 9$ by default unless it is specified).

Searching settings. The original architecture is initialized with 2 feature vertices. We perform *network proliferation* for 4 iterations to obtain a sequence of GNN architectures with the size of $\{2, 4, 8, 16\}$. Specifically, we choose SGAS [32] as the search strategy that can differentiate the local supernet to a specific subnet. During the network differentiation, after warming up for 10 epochs, SGAS begins to simultaneously determine one node-learning operation and one relation-mining operation for every 5 epochs. Thus, the search epoch is set to $\{25, 25, 45, 85\}$ for 4 sequential iterations. To carry out the architecture search, we hold out half of the training data as the validation set. For one-shot differentiable search strategies (SGAS [32] and DARTS [40]), there are operation weights w and architectural parameters α to be optimized. We use momentum SGD to optimize the weights w , with initial learning rate $\eta_w = 0.025$ (annealed down to zero following a cosine schedule without restart), momentum 0.9, and weight

Table 1. **Comparison with state-of-the-art architectures on the CLUSTER, ZINC, CIFAR10 and TSP datasets.** \textcircled{m} denotes the architecture is manually designed. The indicator **E** denotes whether the architecture can learn edge feature. The ARGNP without edge feature means that the relation space is removed from relation-aware graph search space. Note that mean and standard deviation are computed across 4 independently searched GNN architectures.

Architecture	Node Level				Graph Level						Edge Level		
	E \checkmark	CLUSTER			ZINC			CIFAR10			TSP		
		Metric (AA %) \uparrow	Params (M)	Search (day)	Metric (MAE) \downarrow	Params (M)	Search (day)	Metric (OA %) \uparrow	Params (M)	Search (day)	Metric (F1) \uparrow	Params (M)	Search (day)
GCN [29]	\times	68.50 \pm 0.98	0.50	\textcircled{m}	0.367 \pm 0.011	0.50	\textcircled{m}	56.34 \pm 0.38	0.10	\textcircled{m}	0.630 \pm 0.001	0.10	\textcircled{m}
GIN [59]	\times	64.72 \pm 1.55	0.52	\textcircled{m}	0.526 \pm 0.051	0.51	\textcircled{m}	55.26 \pm 1.53	0.10	\textcircled{m}	0.656 \pm 0.003	0.10	\textcircled{m}
GraphSage [21]	\times	63.84 \pm 0.11	0.50	\textcircled{m}	0.398 \pm 0.002	0.51	\textcircled{m}	65.77 \pm 0.31	0.10	\textcircled{m}	0.665 \pm 0.003	0.10	\textcircled{m}
GAT [53]	\times	70.59 \pm 0.45	0.53	\textcircled{m}	0.384 \pm 0.007	0.53	\textcircled{m}	64.22 \pm 0.46	0.11	\textcircled{m}	0.671 \pm 0.002	0.10	\textcircled{m}
GatedGCN [9]	\checkmark	76.08 \pm 0.34	0.50	\textcircled{m}	0.214 \pm 0.013	0.51	\textcircled{m}	67.31 \pm 0.31	0.10	\textcircled{m}	0.838 \pm 0.002	0.53	\textcircled{m}
PNA [15]	\times	N/A	N/A	N/A	0.320 \pm 0.032	0.39	\textcircled{m}	70.46 \pm 0.44	0.11	\textcircled{m}	N/A	N/A	N/A
PNA [15]	\checkmark	N/A	N/A	N/A	0.188 \pm 0.004	0.39	\textcircled{m}	70.47 \pm 0.72	0.11	\textcircled{m}	N/A	N/A	N/A
DGN [5]	\times	N/A	N/A	N/A	0.219 \pm 0.010	0.39	\textcircled{m}	72.70 \pm 0.54	0.11	\textcircled{m}	N/A	N/A	N/A
DGN [5]	\checkmark	N/A	N/A	N/A	0.168 \pm 0.003	0.39	\textcircled{m}	72.84 \pm 0.42	0.11	\textcircled{m}	N/A	N/A	N/A
GNAS-MP [12]	\times	74.77 \pm 0.15	1.61	0.80	0.242 \pm 0.005	1.20	0.40	70.10 \pm 0.44	0.43	3.20	0.742 \pm 0.002	1.20	2.10
ARGNP (2)	\times	61.61 \pm 0.27	0.07	0.04	0.430 \pm 0.003	0.09	0.01	66.55 \pm 0.13	0.10	0.11	0.655 \pm 0.003	0.09	0.05
ARGNP (4)	\times	64.06 \pm 0.45	0.14	0.07	0.303 \pm 0.013	0.14	0.01	66.65 \pm 0.39	0.18	0.14	0.668 \pm 0.003	0.17	0.06
ARGNP (8)	\times	68.73 \pm 0.12	0.25	0.20	0.239 \pm 0.009	0.27	0.02	67.37 \pm 0.32	0.33	0.48	0.674 \pm 0.002	0.29	0.21
ARGNP (16)	\times	71.92 \pm 0.29	0.53	0.71	0.221 \pm 0.004	0.51	0.06	67.10 \pm 0.51	0.58	1.77	0.684 \pm 0.002	0.56	0.76
ARGNP (2)	\checkmark	64.99 \pm 0.31	0.08	0.06	0.318 \pm 0.009	0.08	0.01	69.14 \pm 0.30	0.10	0.17	0.773 \pm 0.001	0.08	0.08
ARGNP (4)	\checkmark	74.75 \pm 0.25	0.15	0.09	0.197 \pm 0.006	0.15	0.01	71.83 \pm 0.32	0.17	0.23	0.821 \pm 0.001	0.14	0.10
ARGNP (8)	\checkmark	76.32 \pm 0.03	0.29	0.31	0.155 \pm 0.003	0.28	0.04	73.72 \pm 0.32	0.33	0.84	0.841 \pm 0.001	0.30	0.39
ARGNP (16)	\checkmark	77.35\pm0.05	0.52	1.10	0.136\pm0.002	0.52	0.15	73.90\pm0.15	0.64	2.95	0.855\pm0.001	0.62	1.23

decay 3×10^{-4} . We use Adam [28] as the optimizer for α , with initial learning rate $\eta_\alpha = 3 \times 10^{-4}$, momentum $\beta = (0.5, 0.999)$ and weight decay 10^{-3} .

Training settings. We follow all the training settings (data splits, optimizer, metrics, *etc.*) in work [12, 17]. Specifically, we adopt Adam [28] with the same learning rate decay for all runs. The learning rate is initialized with 10^{-3} , which is reduced by half if the validation loss stops decreasing after 20 epochs. The weight decay is set to 0. The dropout is set to 0.5 to alleviate the overfitting. Our architectures are all trained for 400 epochs with a batch size of 32. We report the mean and standard deviation of the metric on the test dataset of 4 discovered architectures. These experiments are run on a single NVIDIA GeForce RTX 3090 GPU.

4.2. Results and Analysis

In Table 1 and Table 2, we compare our ARGNP with the state-of-the-art hand-crafted and search-based GNN architectures on the CLUSTER, ZINC, CIFAR10, TSP, ModelNet10, and ModelNet40 datasets. The evaluation metric is the average accuracy (AA) for CLUSTER, mean absolute error (MAE) for ZINC, F1-score (F1) for TSP. For CIFAR10, ModelNet10, and ModelNet40, we use the overall accuracy (OA) as the evaluation metric. To make a fair comparison, we also report the architecture parameters, the search cost, and the mean and standard deviation of all the metrics. We can see that, on all the six datasets for four classical graph learning tasks, the GNN architec-

tures discovered by our ARGNP surpass the state-of-the-art architectures by a large margin in terms of both mean and standard deviation. Compared with the state-of-the-art search-based method GNAS-MP [12], our searched architecture can easily achieve better performance with only $\frac{1}{10} \sim \frac{1}{4}$ parameters. This benefits from that the relation-aware graph search space can mine hierarchical relation information (such as local structural similarity) to guide anisotropic message passing. Moreover, the network proliferation search paradigm can efficiently and effectively explore the proposed search space. We visualize the best-performed GNN architecture with the size of 4 in Figure 5, which is searched on the ModelNet40 dataset. Other examples are provided in the supplementary material.

4.3. Ablation of Search Space

We study the influence of the relation search space in our proposed relation-aware graph search. First, we construct a search space variant by removing the relation search space. Then we perform GNN architecture search on this variant using the network proliferation search paradigm and obtain a sequence of GNN architectures with the size of $\{2, 4, 8, 16\}$. These GNN architectures are evaluated on six datasets. For a fair comparison, we increase the dimension of the node features to keep the architectural parameters comparable. As shown in Table 1 and Table 2, the best performance of the search space variant without relation learning descends by a large margin. Under all the differ-

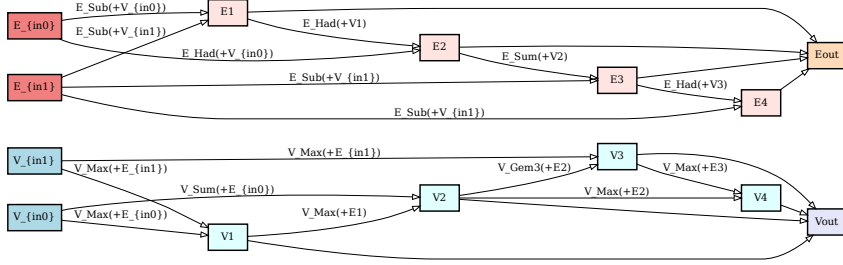


Figure 5. The best GNN architecture with the network size of 4 searched on the ModelNet40 dataset.

Table 2. Comparison with state-of-the-art architectures on the ModelNet10 and ModelNet40 datasets at 3D point cloud recognition task. L denotes the size of GNN architecture.

Architecture	ModelNet10		ModelNet40		Params (M)	Search (Day)
	L (#)	E (✓)	Metric (OA %) ↑	Metric (OA %) ↑		
3DmFV [6]	/	/	95.2	91.6	45.77	Ⓜ
PointNet++ [47]	/	/	N/A	90.7	1.48	Ⓜ
PCNN [3]	/	/	N/A	92.3	8.20	Ⓜ
PointCNN [35]	/	/	N/A	92.2	0.60	Ⓜ
DGCNN [55]	/	/	N/A	92.2	1.84	Ⓜ
KPConv [52]	/	/	N/A	92.9	14.3	Ⓜ
SGAS [32]	9	✓	N/A	92.93±0.19	8.87	0.19
ARGNP	2 ×	✓	93.20±0.24	91.11±0.24	1.80	0.03
ARGNP	4 ×	✓	93.86±0.25	91.30±0.22	2.27	0.04
ARGNP	8 ×	✓	94.23±0.22	91.85±0.18	3.20	0.15
ARGNP	2	✓	95.07±0.31	92.47±0.23	2.50	0.04
ARGNP	4	✓	95.35±0.23	92.80±0.19	3.05	0.06
ARGNP	8	✓	95.87±0.22	93.33±0.15	4.15	0.20

ent network size settings, relation learning can significantly improve the capability of graph reasoning. Interestingly, this improvement is also observed on the CLUSTER, CIFAR10, and ModelNet datasets which don’t have original edge features. Taking the CLUSTER dataset as an example, it aims at identifying the community clusters, where the graphs represent the community networks. The edges play a role in connecting two nodes and have no original meaningful features. In this case, relation learning can mine hierarchical relational information by extracting local structural similarities between nodes. This can help distinguish between intra-community and extra-community connections for learning better discriminative node features.

4.4. Ablation of Search Paradigm

To investigate the effectiveness of our *Network Proliferation Search Paradigm (NPSP)*, we conduct the ablation experiments on ZINC dataset around *network size*, *search strategy*, *whether to use cell trick* and *whether to use NPSP*. We run 14 different experiments and report the results in Table 3. We observe the following phenomena. First, *the cell trick improves the search efficiency but weakens the expressive capability of graph search space*. This results from its

Table 3. Performance of the relation-aware graph search space under different settings. Cell is an indicator of whether to use the cell trick. NPSP is an indicator of whether to use the network proliferation search. OOM denotes out of memory.

#	Method	ZINC						
		L (#)	Search Strategy	Cell (✓)	NPSP (✓)	Metric (MAE) ↓	Params (M)	Search (Day)
1	R-space	8	Random	×	×	0.303±0.058	0.27	0.
2	R-space	8	DARTS	✓	×	0.160±0.005	0.28	0.17
3	R-space	8	DARTS	×	×	0.157±0.008	0.28	0.30
4	R-space	8	DARTS	×	✓	0.150±0.006	0.29	0.08
5	R-space	8	SGAS	✓	×	0.165±0.008	0.30	0.13
6	R-space	8	SGAS	×	×	0.161±0.008	0.30	0.25
7	R-space	8	SGAS	×	✓	0.155±0.003	0.28	0.06
8	R-space	16	Random	×	×	0.185±0.024	0.51	0.
9	R-space	16	DARTS	✓	×	0.144±0.004	0.57	0.38
10	R-space	16	DARTS	×	×	N/A	N/A	OOM
11	R-space	16	DARTS	×	✓	0.139±0.005	0.56	0.24
12	R-space	16	SGAS	✓	×	0.140±0.003	0.60	0.32
13	R-space	16	SGAS	×	×	N/A	N/A	OOM
14	R-space	16	SGAS	×	✓	0.136±0.002	0.52	0.21

original assumption where the GNN architecture is a stack of the same building cells that narrows our relation-aware graph search space. Therefore, the search strategy with the cell trick performs worse than that without it, which is demonstrated by the contrast between exp 2 and exp 3, exp 5 and exp 6. Second, our *NPSP can both significantly improve the search efficiency and search effect with different search strategies*. The performance improvement benefits from that the *NPSP* can alleviate the subnet interference and mitigate the shrink of search space by breaking away from the cell assumption. The efficiency improvement lies in that *NPSP* shifts the training object from global supernet to sequential local supernets. They are supported by exp 4, 7, 11, and 14, where *NPSP* achieves the best performance with less time cost under all the experimental settings.

4.5. Visualizing Hierarchical Features

To better demonstrate the effectiveness of the relation learning, we provide relation and node features visualization on ModelNet40 dataset. During the inference, we feed forward one 3D pointcloud object into the network with

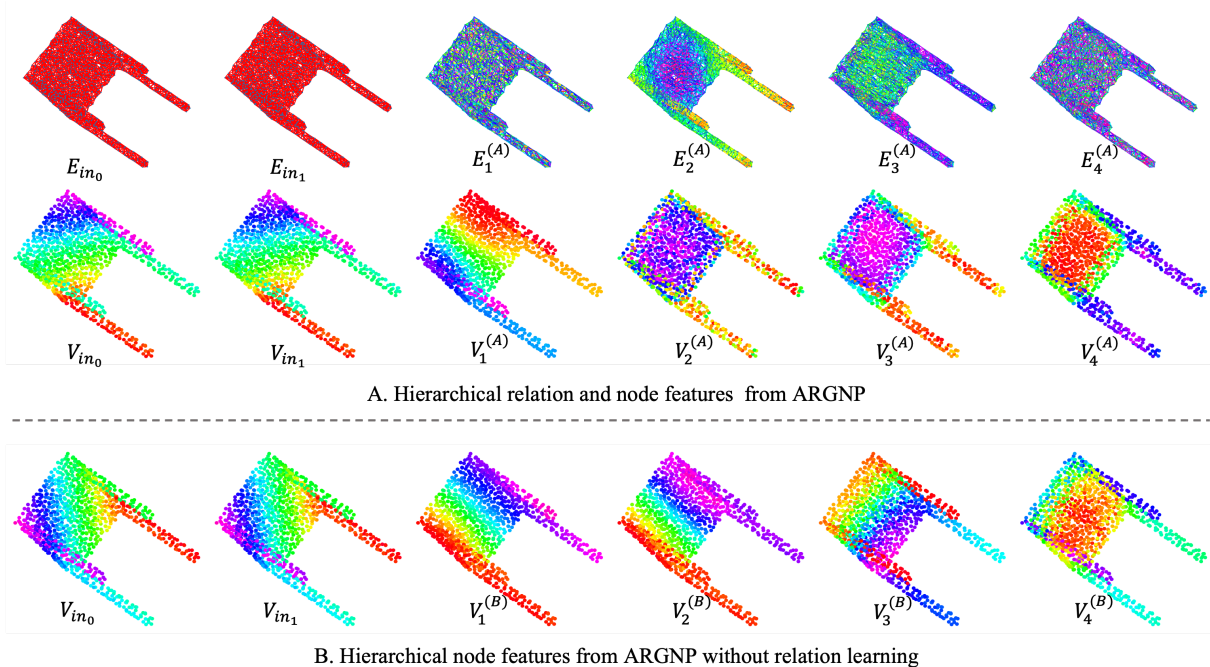


Figure 6. **Visualization of the learned hierarchical features for 3D point cloud recognition** (taking table as an example). Relation features with different edge color distribution have different message passing preferences. Node features with different node color distribution represent different clustering effects.

the input $\{V_{in_0}, V_{in_1}, E_{in_0}, E_{in_1}\}$, where $V_{in_0} = V_{in_1} \in \mathbb{R}^{1024 \times 3}$ are the 3D coordinates and $E_{in_0} = E_{in_1} = \mathbf{1} \in \mathbb{R}^{(1024 \times 9) \times 1}$ are the pseudo relation features. The hierarchical node/relation features generated from each layer is denoted as $\{V_1, \dots, V_4\}$ and $\{E_1, \dots, E_4\}$, respectively. For better visualization on the point cloud graph, we reduce the feature dimension to 1 through principal component analysis (PCA). The edges with a similar color are considered to have the same message passing preferences, while the nodes with a similar color are considered to belong to a similar cluster. A visualization example from ARGNP and a version without relation learning architecture are shown in Figure 6A and 6B, respectively.

As shown in Figure 6A, ARGNP can capture the structural information and well discriminate different parts of the object (e.g., the legs, desktop, and border of the table in $V_4^{(A)}$). In contrast, as shown in Figure 6B, the original GNN without relation learning architecture can only gradually propagate the node information through the input graph based on 3D coordinates. As a result, the similar nodes that are distant in the 3D space can not be well clustered (e.g., 4 legs of the table in $V_4^{(B)}$). The above comparison shows that the relation features can guide better message passing mechanisms to learn more effective node features. To show the role of the relation learning more specifically, accompanied with the searched GNN in Figure 5, we analyze the features in Figure 6A. For example, the $E_1^{(A)}$ is learned by

substraction operation. The *substraction* operation is similar to an “border detection” operation that can discriminate the directions between two nodes. In this way, the ARGNP can directly distinguish groups of parallel components of an object (e.g., legs, parallel borders, etc. in $V_2^{(A)}$). However, without using the relation features, it requires numerous rounds of message passing which may cause the over smoothing problem. With the help of relation learning, the components with similar structures can be well clustered.

5. Conclusion

This paper proposes the automatic relation-aware graph network proliferation (ARGNP) method to design the optimal GNN architectures by devising a novel relation-aware graph search space and a network proliferation search paradigm. The search space significantly improves the upper bound of the discovered GNN’s reasoning capability while the proliferation search paradigm promotes search efficiency and effectiveness. Experiments show that ARGNP achieves superior performance for four tasks on six datasets.

Acknowledgement. This work was supported in part by the National Key R&D Program of China under Grant 2018AAA0102000, and in part by the National Natural Science Foundation of China: U21B2038, 61931008, 61732007, and CAAI-Huawei MindSpore Open Fund, Youth Innovation Promotion Association of CAS under Grant 2020108, CCF-Baidu Open Fund.

References

- [1] Emmanuel Abbe. Community detection and stochastic block models: recent developments. *The Journal of Machine Learning Research*, 18(1):6446–6531, 2017. **5**
- [2] Radhakrishna Achanta, Appu Shaji, Kevin Smith, Aurelien Lucchi, Pascal Fua, and Sabine Süsstrunk. Slic superpixels compared to state-of-the-art superpixel methods. *IEEE transactions on pattern analysis and machine intelligence*, 34(11):2274–2282, 2012. **5**
- [3] Matan Atzmon, Haggai Maron, and Yaron Lipman. Point convolutional neural networks by extension operators. *ACM Transactions on Graphics (TOG)*, 37:1–12, 2018. **7**
- [4] Bowen Baker, Otkrist Gupta, Nikhil Naik, and Ramesh Raskar. Designing neural network architectures using reinforcement learning. *arXiv preprint arXiv:1611.02167*, 2016. **2**
- [5] Dominique Beaini, Saro Passaro, Vincent L’etourneau, William L. Hamilton, Gabriele Corso, and Pietro Lio’. Directional graph networks. In *ICML*, 2021. **6**
- [6] Yizhak Ben-Shabat, Michael Lindenbaum, and Anath Fischer. 3dmfv: Three-dimensional point cloud classification in real-time using convolutional neural networks. *IEEE Robotics and Automation Letters*, 3:3145–3152, 2018. **7**
- [7] Maxim Berman, Hervé Jégou, Andrea Vedaldi, Iasonas Kokkinos, and Matthijs Douze. Multigrain: a unified image embedding for classes and instances. *ArXiv*, abs/1902.05509, 2019. **12**
- [8] Giorgos Bouritsas, Fabrizio Frasca, Stefanos Zafeiriou, and Michael M. Bronstein. Improving graph neural network expressivity via subgraph isomorphism counting. *ArXiv*, abs/2006.09252, 2020. **1**
- [9] Xavier Bresson and Thomas Laurent. Residual gated graph convnets. *ArXiv*, abs/1711.07553, 2017. **2, 6**
- [10] Marc Brockschmidt. Gnn-film: Graph neural networks with feature-wise linear modulation. In *ICML*, 2020. **2, 3**
- [11] Han Cai, Ligeng Zhu, and Song Han. Proxylessnas: Direct neural architecture search on target task and hardware. *arXiv preprint arXiv:1812.00332*, 2018. **2**
- [12] Shaofei Cai, Liang Li, Jincan Deng, Beichen Zhang, Zhengjun Zha, Li Su, and Qingming Huang. Rethinking graph neural architecture search from message-passing. In *CVPR*, 2021. **1, 2, 3, 5, 6**
- [13] Xin Chen, Lingxi Xie, Jingjing Wu, and Qi Tian. Progressive differentiable architecture search: Bridging the depth gap between search and evaluation. *2019 IEEE/CVF International Conference on Computer Vision (ICCV)*, pages 1294–1303, 2019. **5**
- [14] Xiangxiang Chu, Xiaoxing Wang, Bo Zhang, Shun Lu, Xiaolin Wei, and Junchi Yan. Darts-: robustly stepping out of performance collapse without indicators. *arXiv preprint arXiv:2009.01027*, 2020. **2**
- [15] Gabriele Corso, Luca Cavalleri, Dominique Beaini, Pietro Lio’, and Petar Velickovic. Principal neighbourhood aggregation for graph nets. *NIPS*, 2020. **2, 5, 6, 12**
- [16] Vijay Prakash Dwivedi, Chaitanya K. Joshi, Thomas Laurent, Yoshua Bengio, and Xavier Bresson. Benchmarking graph neural networks. *ArXiv*, abs/2003.00982, 2020. **1**
- [17] Vijay Prakash Dwivedi, Chaitanya K Joshi, Thomas Laurent, Yoshua Bengio, and Xavier Bresson. Benchmarking graph neural networks. *arXiv preprint arXiv:2003.00982*, 2020. **5, 6, 13**
- [18] Yang Gao, Hong Yang, Peng Zhang, Chuan Zhou, and Yue Hu. Graph neural architecture search. In *IJCAI*, 2020. **1, 2**
- [19] Justin Gilmer, Samuel S. Schoenholz, Patrick F. Riley, Oriol Vinyals, and George E. Dahl. Neural message passing for quantum chemistry. *ArXiv*, abs/1704.01212, 2017. **1**
- [20] Jiayuan Gu, Han Hu, Liwei Wang, Yichen Wei, and Jifeng Dai. Learning region features for object detection. In *Proceedings of the european conference on computer vision (ECCV)*, pages 381–395, 2018. **1**
- [21] William L. Hamilton, Zhitao Ying, and Jure Leskovec. Inductive representation learning on large graphs. In *NIPS*, 2017. **2, 6, 12**
- [22] Chaoyang He, Haishan Ye, Li Shen, and Tong Zhang. Milenas: Efficient neural architecture search via mixed-level reformulation. *2020 IEEE/CVF Conference on Computer Vision and Pattern Recognition (CVPR)*, pages 11990–11999, 2020. **5**
- [23] Han Hu, Jiayuan Gu, Zheng Zhang, Jifeng Dai, and Yichen Wei. Relation networks for object detection. In *Proceedings of the IEEE conference on computer vision and pattern recognition*, pages 3588–3597, 2018. **1**
- [24] Han Hu, Deyi Ji, Weihao Gan, Shuai Bai, Wei Wu, and Junjie Yan. Class-wise dynamic graph convolution for semantic segmentation. In *ECCV*, 2020. **1**
- [25] Md Shamim Hussain, Mohammed J. Zaki, and D. Subramanian. Edge-augmented graph transformers: Global self-attention is enough for graphs. *ArXiv*, abs/2108.03348, 2021. **1**
- [26] John J Irwin, Teague Sterling, Michael M Mysinger, Erin S Bolstad, and Ryan G Coleman. Zinc: a free tool to discover chemistry for biology. *Journal of chemical information and modeling*, 52(7):1757–1768, 2012. **5**
- [27] Jongmin Kim, Taesup Kim, Sungwoon Kim, and Chang Dong Yoo. Edge-labeling graph neural network for few-shot learning. *2019 IEEE/CVF Conference on Computer Vision and Pattern Recognition (CVPR)*, pages 11–20, 2019. **1**
- [28] Diederik P. Kingma and Jimmy Ba. Adam: A method for stochastic optimization. *CoRR*, abs/1412.6980, 2015. **6**
- [29] Thomas Kipf and Max Welling. Semi-supervised classification with graph convolutional networks. *ArXiv*, abs/1609.02907, 2017. **2, 6, 13**
- [30] Alex Krizhevsky, Geoffrey Hinton, et al. Learning multiple layers of features from tiny images. 2009. **5**
- [31] Loic Landrieu and Martin Simonovsky. Large-scale point cloud semantic segmentation with superpoint graphs. In *Proceedings of the IEEE conference on computer vision and pattern recognition*, pages 4558–4567, 2018. **1**
- [32] Guohao Li, Guocheng Qian, Itzel C Delgadillo, Matthias Muller, Ali Thabet, and Bernard Ghanem. Sgas: Sequential greedy architecture search. In *Proceedings of the IEEE/CVF Conference on Computer Vision and Pattern Recognition*, pages 1620–1630, 2020. **1, 2, 5, 7, 12, 13, 14**

- [33] G. Li, Guocheng Qian, Itzel C. Delgadillo, Matthias Müller, Ali K. Thabet, and Bernard Ghanem. Sgas: Sequential greedy architecture search. *2020 IEEE/CVF Conference on Computer Vision and Pattern Recognition (CVPR)*, pages 1617–1627, 2020. [1](#), [2](#), [3](#), [5](#)
- [34] Xia Li, Yibo Yang, Qijie Zhao, Tiancheng Shen, Zhouchen Lin, and Hong Liu. Spatial pyramid based graph reasoning for semantic segmentation. *2020 IEEE/CVF Conference on Computer Vision and Pattern Recognition (CVPR)*, pages 8947–8956, 2020. [1](#)
- [35] Yangyan Li, Rui Bu, Mingchao Sun, Wei Wu, Xinhan Di, and Baoquan Chen. Pointcnn: Convolution on x-transformed points. In *NeurIPS*, 2018. [7](#)
- [36] Yangyang Li, Yipeng Ji, Shaoning Li, Shulong He, Yincao Cao, Xiong Li, Jun Shi, Yangchao Yang, and Yifeng Liu. Relevance-aware anomalous users detection in social network via graph neural network. *2021 International Joint Conference on Neural Networks (IJCNN)*, pages 1–8, 2021. [1](#)
- [37] Yanxi Li, Zean Wen, Yunhe Wang, and Chang Xu. One-shot graph neural architecture search with dynamic search space. In *AAAI*, 2021. [1](#), [2](#), [3](#)
- [38] Hanwen Liang, Shifeng Zhang, Jiacheng Sun, Xingqiu He, Weiran Huang, Kechen Zhuang, and Zhenguo Li. Darts+: Improved differentiable architecture search with early stopping. *arXiv preprint arXiv:1909.06035*, 2019. [2](#)
- [39] Hanxiao Liu, Karen Simonyan, Oriol Vinyals, Chrisantha Fernando, and Koray Kavukcuoglu. Hierarchical representations for efficient architecture search. *arXiv preprint arXiv:1711.00436*, 2017. [2](#)
- [40] Hanxiao Liu, Karen Simonyan, and Yiming Yang. Darts: Differentiable architecture search. *ArXiv*, abs/1806.09055, 2019. [2](#), [3](#), [5](#), [14](#)
- [41] Yujia Liu, Kang Zeng, Haiyang Wang, Xin Song, and Bin Zhou. Content matters: A gnn-based model combined with text semantics for social network cascade prediction. In *PAKDD*, 2021. [1](#)
- [42] Diego Marcheggiani and Ivan Titov. Encoding sentences with graph convolutional networks for semantic role labeling. *arXiv preprint arXiv:1703.04826*, 2017. [2](#)
- [43] Federico Monti, Davide Boscaini, Jonathan Masci, Emanuele Rodola, Jan Svoboda, and Michael M Bronstein. Geometric deep learning on graphs and manifolds using mixture model cnns. In *Proceedings of the IEEE conference on computer vision and pattern recognition*, pages 5115–5124, 2017. [2](#)
- [44] Zheyi Pan, Songyu Ke, Xiaodu Yang, Yuxuan Liang, Yong Yu, Junbo Zhang, and Yu Zheng. Autostg: Neural architecture search for predictions of spatio-temporal graph. *Proceedings of the Web Conference 2021*, 2021. [1](#), [2](#)
- [45] Pietro Perona and Jitendra Malik. Scale-space and edge detection using anisotropic diffusion. *IEEE Transactions on pattern analysis and machine intelligence*, 12(7):629–639, 1990. [2](#)
- [46] Hieu Pham, Melody Guan, Barret Zoph, Quoc Le, and Jeff Dean. Efficient neural architecture search via parameters sharing. In *International Conference on Machine Learning*, pages 4095–4104. PMLR, 2018. [2](#)
- [47] C. Qi, L. Yi, Hao Su, and Leonidas J. Guibas. Pointnet++: Deep hierarchical feature learning on point sets in a metric space. In *NIPS*, 2017. [7](#)
- [48] Xiaojuan Qi, Renjie Liao, Jiaya Jia, Sanja Fidler, and Raquel Urtasun. 3d graph neural networks for rgb-d semantic segmentation. In *Proceedings of the IEEE International Conference on Computer Vision*, pages 5199–5208, 2017. [1](#)
- [49] Esteban Real, Alok Aggarwal, Yanping Huang, and Quoc V Le. Regularized evolution for image classifier architecture search. In *Proceedings of the aaai conference on artificial intelligence*, volume 33, pages 4780–4789, 2019. [2](#)
- [50] Esteban Real, Sherry Moore, Andrew Selle, Saurabh Saxena, Yutaka Leon Suematsu, Jie Tan, Quoc V Le, and Alexey Kurakin. Large-scale evolution of image classifiers. In *International Conference on Machine Learning*, pages 2902–2911. PMLR, 2017. [2](#)
- [51] Victor Garcia Satorras and Joan Bruna. Few-shot learning with graph neural networks. *ArXiv*, abs/1711.04043, 2018. [1](#)
- [52] Hugues Thomas, C. Qi, Jean-Emmanuel Deschaud, Beatriz Marcotequi, François Goulette, and Leonidas J. Guibas. Kpconv: Flexible and deformable convolution for point clouds. *2019 IEEE/CVF International Conference on Computer Vision (ICCV)*, pages 6410–6419, 2019. [7](#)
- [53] Petar Velickovic, Guillem Cucurull, Arantxa Casanova, Adriana Romero, Pietro Lio, and Yoshua Bengio. Graph attention networks. *ArXiv*, abs/1710.10903, 2018. [2](#), [6](#), [13](#)
- [54] Lei Wang, Yuchun Huang, Yaolin Hou, Shenman Zhang, and Jie Shan. Graph attention convolution for point cloud semantic segmentation. *2019 IEEE/CVF Conference on Computer Vision and Pattern Recognition (CVPR)*, pages 10288–10297, 2019. [1](#)
- [55] Yue Wang, Yongbin Sun, Ziwei Liu, Sanjay E Sarma, Michael M Bronstein, and Justin M Solomon. Dynamic graph cnn for learning on point clouds. *Acm Transactions On Graphics (tog)*, 38(5):1–12, 2019. [1](#), [7](#)
- [56] Zhirong Wu, Shuran Song, Aditya Khosla, Fisher Yu, Linguang Zhang, Xiaoou Tang, and Jianxiong Xiao. 3d shapenets: A deep representation for volumetric shapes. *2015 IEEE Conference on Computer Vision and Pattern Recognition (CVPR)*, pages 1912–1920, 2015. [5](#)
- [57] Sirui Xie, Hehui Zheng, Chunxiao Liu, and Liang Lin. Snas: stochastic neural architecture search. *arXiv preprint arXiv:1812.09926*, 2018. [2](#)
- [58] Sirui Xie, Hehui Zheng, Chunxiao Liu, and Liang Lin. Snas: Stochastic neural architecture search. *ArXiv*, abs/1812.09926, 2019. [5](#)
- [59] Keyulu Xu, Weihua Hu, Jure Leskovec, and Stefanie Jegelka. How powerful are graph neural networks? *ArXiv*, abs/1810.00826, 2019. [2](#), [3](#), [6](#), [12](#), [13](#)
- [60] Yuhui Xu, Lingxi Xie, Xiaopeng Zhang, Xin Chen, Guo-Jun Qi, Qi Tian, and Hongkai Xiong. Pc-darts: Partial channel connections for memory-efficient differentiable architecture search. *ArXiv*, abs/1907.05737, 2019. [2](#), [5](#)
- [61] Ling Yang, Liangliang Li, Zilu Zhang, Xinyu Zhou, Erjin Zhou, and Y. W. Liu. Dpgn: Distribution propagation graph network for few-shot learning. *2020 IEEE/CVF Conference on Computer Vision and Pattern Recognition (CVPR)*, pages 13387–13396, 2020. [1](#)

- [62] Yiding Yang, Zunlei Feng, Mingli Song, and Xinchao Wang. Factorizable graph convolutional networks. *Advances in Neural Information Processing Systems*, 33, 2020. [2](#)
- [63] Yuge Zhang, Zejun Lin, Junyan Jiang, Quanlu Zhang, Yujing Wang, Hui Xue, Chen Zhang, and Yaming Yang. Deeper insights into weight sharing in neural architecture search. *ArXiv*, abs/2001.01431, 2020. [2](#)
- [64] Yuge Zhang, Chenqian Yan, Quanlu Zhang, Li Lyna Zhang, Yaming Yang, Xiaotian Gao, and Yuqing Yang. Acenas: Learning to rank ace neural architectures with weak supervision of weight sharing. *ArXiv*, abs/2108.03001, 2021. [2](#)
- [65] Huan Zhao, Lanning Wei, and Quanming Yao. Simplifying architecture search for graph neural network. *ArXiv*, abs/2008.11652, 2020. [1](#), [2](#)
- [66] Kaixiong Zhou, Qingquan Song, Xiao Huang, and Xia Hu. Auto-gnn: Neural architecture search of graph neural networks. *ArXiv*, abs/1909.03184, 2019. [1](#), [2](#)
- [67] Barret Zoph and Quoc V Le. Neural architecture search with reinforcement learning. *arXiv preprint arXiv:1611.01578*, 2016. [2](#)

A. Search Space Details

In this section, we first detail how node-learning operations and relation-learning operations are formulated. Then we introduce the design of task-based layers for different graph learning tasks. $\mathbf{V} \in \mathbb{R}^{n \times d_V}$, $\mathbf{E} \in \mathbb{R}^{m \times d_E}$ are node features and relation features that are fed forward to node-learning and relation-learning operations, respectively. n and m are the number of nodes and edges of the input graph data.

A.1. Node-learning Operations

As discussed in the body content, a node-learning operation $\mathcal{O}_{\mathcal{V}}^{(i,j)}$ computes the transformed information from feature vertex \mathbf{V}_i to \mathbf{V}_j , which is denoted as $\mathbf{V}_{i \rightarrow j} = \mathcal{O}_{\mathcal{V}}^{(i,j)}(\mathbf{V}_i, \mathbf{E}_i, f_{i,j})$. Specifically, given node t on the graph, its transformed node feature $\mathbf{V}_{i \rightarrow j}^t$ is formulated as

$$\mathbf{V}_{i \rightarrow j}^t = f_{i,j}(\{\gamma_{s,t} \odot \mathbf{V}_i^s + \beta_{s,t} | s \in \mathcal{N}(t)\}), \quad (4)$$

$$\gamma_{s,t}, \beta_{s,t} = g(\mathbf{E}_i^{s,t}; \boldsymbol{\theta}),$$

where, $\mathcal{N}(t)$ denotes the set of neighbors of target node t on the graph, $f_{i,j}$ is an aggregating function. $g(\cdot)$ is a two-layer multilayer perceptron to compute the affine transformation with the learnable parameters $\boldsymbol{\theta} = [\mathbf{W}^1 \ \mathbf{W}^2 \ \mathbf{W}^k \ \mathbf{W}^b]$, which is formulated as

$$[\gamma_{s,t} \ \beta_{s,t}] = \sigma(\sigma(\mathbf{E}_i^{s,t} \mathbf{W}^1) \mathbf{W}^2) [\mathbf{W}^k \ \mathbf{W}^b], \quad (5)$$

where $\sigma(\cdot)$ is the rectified linear unit. The difference between different node-learning operations lies in the choice of message aggregating functions. We design 8 candidate aggregating function options, *i.e.*, V_MEAN , V_SUM , V_MAX , V_STD , V_GEM2 , V_GEM3 , $zero$ and $skip-connect$ for capturing different types of information. For clarity, we denote $\mathbf{M}_{s,t}$ as the modulated incoming message from node t to node s , where $\mathbf{M}_{s,t} = \gamma_{s,t} \odot \mathbf{V}_i^s + \beta_{s,t}$. The mean aggregation of neighboring messages is denoted as

$$\mu_t(\mathbf{M}) = \frac{1}{|\mathcal{N}(t)|} \sum_{s \in \mathcal{N}(t)} \mathbf{M}_{s,t}. \quad (6)$$

V_MEAN is the average of neighboring messages, which captures the mean statistics of neighboring messages [21], written as

$$\mathbf{V}_{i \rightarrow j}^t = \mu_t(\mathbf{M}). \quad (7)$$

V_SUM is the sum of neighboring messages, which captures local structural information [59], written as

$$\mathbf{V}_{i \rightarrow j}^t = |\mathcal{N}(t)| \times \mu_t(\mathbf{M}). \quad (8)$$

V_MAX is the max of neighboring messages, which captures the representative information [59], written as

$$\mathbf{V}_{i \rightarrow j}^t = \max_{s \in \mathcal{N}(t)} \mathbf{M}_{s,t}. \quad (9)$$

V_STD is the standard deviation of input feature set, which captures the stability of neighboring messages [15], *i.e.*,

$$\mathbf{V}_{i \rightarrow j}^t = \sqrt{ReLU(\mu_t(\mathbf{M}^2) - \mu_t(\mathbf{M}))} + \epsilon, \quad (10)$$

where $ReLU$ is the rectified linear unit used to avoid negative values caused by numerical errors and ϵ is a small positive number to ensure the output is differentiable [15].

Moreover, we also introduce Generalized Mean Pooling (GeM) for aggregating messages, which can focus on learning to propagate the prominent message [7], written as

$$GeM_t(\mathbf{M}, \alpha) = \sqrt[\alpha]{ReLU(\mu_t(\mathbf{M}^\alpha))} + \epsilon, \quad (11)$$

where α is the hyper parameter. Here, we adopt two widely used parameters to construct the node-learning operations, *i.e.*, V_GEM2 and V_GEM3 .

V_GEM2 :

$$\mathbf{V}_{i \rightarrow j}^t = GeM_t(\mathbf{M}, 2). \quad (12)$$

V_GEM3 :

$$\mathbf{V}_{i \rightarrow j}^t = GeM_t(\mathbf{M}, 3). \quad (13)$$

$skip-connect$ is to enhance the central node information and mitigate the gradient vanishing, written as

$$\mathbf{V}_{i \rightarrow j}^t = \mathbf{V}_i^t. \quad (14)$$

$zero$ operation is included in the search space to indicate a lack of connection. Links that are important should have a low weight in the $zero$ operation [32]. It is formulated as

$$\mathbf{V}_{i \rightarrow j}^t = \mathbf{0} \times \mathbf{V}_i^t. \quad (15)$$

A.2. Relation-mining Operations

A relation-mining operation $\mathcal{O}_{\mathcal{E}}^{(i,j)}$ computes the transformed relational information $\mathbf{E}_{i \rightarrow j} = \mathcal{O}_{\mathcal{E}}^{(i,j)}(\mathbf{V}_i, \mathbf{E}_i, h_{i,j})$. $h_{i,j}$ is a relation-mining network, such as *subtraction*, *hardward product*, *gauss kernel*, *etc.* Specifically, given a specific edge (s, t) on the graph, $\mathbf{E}_{i \rightarrow j}^{s,t}$ is computed using feature-wise linear modulation:

$$\mathbf{E}_{i \rightarrow j}^{s,t} = \gamma_{s,t} \odot \mathbf{E}_i^{s,t} + \beta_{s,t}, \quad (16)$$

$$\gamma_{s,t}, \beta_{s,t} = h_{i,j}(\mathbf{V}_i^s, \mathbf{V}_i^t; \boldsymbol{\theta}),$$

$\gamma_{s,t}, \beta_{s,t}$ is the affine transformation learned by $h_{i,j}$ with the learnable parameters $\boldsymbol{\theta} = [\mathbf{W}^1 \ \mathbf{W}^2 \ \mathbf{W}^k \ \mathbf{W}^b]$ and relation function $h^*(\cdot, \cdot)$

$$[\gamma_{s,t} \ \beta_{s,t}] = \sigma(\sigma(h^*(\mathbf{V}_i^s, \mathbf{V}_i^t) \mathbf{W}^1) \mathbf{W}^2) [\mathbf{W}^k \ \mathbf{W}^b], \quad (17)$$

where $\sigma(\cdot)$ is the rectified linear unit. The difference between different relation-mining operations lies in the choice of relation functions $h^*(\cdot, \cdot)$. We design 8 candidate relation functions, *i.e.*, E_SUB , E_GAUSS , E_HAD , E_MAX ,

E_SUM , E_MEAN , $skip-connect$, and $zero$ for capturing different types of relational information.

E_SUB captures the relative change between two nodes. Its relation function is computed as

$$h^*(\mathbf{V}_i^s, \mathbf{V}_i^t) = \mathbf{V}_i^s - \mathbf{V}_i^t \quad (18)$$

E_GAUSS measures the distance between the central node and its neighboring nodes:

$$h^*(\mathbf{V}_i^s, \mathbf{V}_i^t) = \exp\left(\frac{|\mathbf{V}_i^s - \mathbf{V}_i^t|^2}{2\sigma}\right) \quad (19)$$

E_HAD emphasizes on learning the commonalities between the central node and its neighbors:

$$h^*(\mathbf{V}_i^s, \mathbf{V}_i^t) = \mathbf{V}_i^s \odot \mathbf{V}_i^t \quad (20)$$

E_SUM :

$$h^*(\mathbf{V}_i^s, \mathbf{V}_i^t) = \mathbf{V}_i^s + \mathbf{V}_i^t \quad (21)$$

E_MAX :

$$h^*(\mathbf{V}_i^s, \mathbf{V}_i^t) = \max(\mathbf{V}_i^s, \mathbf{V}_i^t) \quad (22)$$

E_MEAN :

$$h^*(\mathbf{V}_i^s, \mathbf{V}_i^t) = \frac{\mathbf{V}_i^s + \mathbf{V}_i^t}{2} \quad (23)$$

$skip-connect$ operation is to enhance the original relational information and mitigate the gradient vanishing, written as

$$[\gamma_{s,t} \quad \beta_{s,t}] = [\mathbf{1} \quad \mathbf{0}] \quad (24)$$

$zero$ operation is included in the search space to indicate a lack of connection. Links that are important should have a low weight in the $zero$ operation [32]. It is formulated as

$$[\gamma_{s,t} \quad \beta_{s,t}] = [\mathbf{0} \quad \mathbf{0}] \quad (25)$$

A.3. Task-based Layer

We design the final network layers depending on the specific task. Suppose there are 8 node feature vertices $\{\mathbf{V}_1, \dots, \mathbf{V}_8\}$ and 8 relation feature vertices $\{\mathbf{E}_1, \dots, \mathbf{E}_8\}$ in our GNN architecture, we compute the global node features \mathbf{V}_g and global edge features \mathbf{E}_g using the following formula

$$\begin{aligned} \mathbf{V}_g &= \sigma(\text{BN}([\mathbf{V}_1 || \dots || \mathbf{V}_8] \mathbf{W}_V)), \\ \mathbf{E}_g &= \sigma(\text{BN}([\mathbf{E}_1 || \dots || \mathbf{E}_8] \mathbf{W}_E)), \end{aligned} \quad (26)$$

where $\mathbf{W}_V \in \mathbb{R}^{d_V \times d_V}$, $\mathbf{W}_E \in \mathbb{R}^{d_E \times d_E}$ are the learnable parameters, BN denotes batch normalization operation, $\sigma(\cdot)$ is the rectified linear unit, $[||\cdot||]$ denotes the feature concatenation operation. The global graph representation \mathbf{G}_g is computed using mean-pooling readout operation over global node features and global edge features, *i.e.*,

$$\mathbf{G}_g = \left[\frac{1}{|\mathbf{V}_g|} \sum_{i \in \mathbf{V}_g} \mathbf{V}_g^i \parallel \frac{1}{|\mathbf{E}_g|} \sum_{(s,t) \in \mathbf{E}_g} \mathbf{E}_g^{s,t} \right], \quad (27)$$

where $|\mathbf{V}_g|$ is the number of nodes, $|\mathbf{E}_g|$ is the number of edges. Notably, this is different from the traditional GNN architecture whose global graph representation is only constructed on the readout of node features. Since our method can learn both node features and relation features, they are all leveraged to construct the global graph representation. This helps the graph representation embeds more useful relational information.

Node-level task layer. For node classification task, the prediction of node i is done as follows

$$\mathbf{y}^i = \mathbf{V}_g^i \mathbf{C}_V, \quad (28)$$

where $\mathbf{C}_V \in \mathbb{R}^{d_V \times n_V}$ is the node classifier, n_V is the number of node classes.

Edge-level task layer. For edge classification task, our method naturally makes prediction based on deep relation features \mathbf{E}_g , formally written as

$$\mathbf{y}^{s,t} = \mathbf{E}_g^{s,t} \mathbf{C}_E, \quad (29)$$

where $\mathbf{C}_E \in \mathbb{R}^{d_E \times n_E}$ is the edge classifier, n_E is the number of edge classes. This is better than traditional GNN works [17, 29, 53, 59] that concatenate the entity features as edge features, since the independent edge features (associated with the relational information) are more discriminative for edge-level tasks.

Graph-level task layer. For graph classification and regression tasks, we make the prediction based on the global graph representation, *i.e.*,

$$\mathbf{y} = \mathbf{G}_g \mathbf{C}_G, \quad (30)$$

where $\mathbf{C}_G \in \mathbb{R}^{(d_V+d_E) \times n_G}$, n_G is the number of graph classes. If it is graph regression task, then $n_G = 1$.

B. Network Differentiation Details

An architecture is represented as a directed acyclic graph (DAG) with $\{\mathbb{V}, \mathbb{L}\}$, where $\mathbb{V} = \{\mathbf{X}_i\}$ is the set of feature vertices and $\mathbb{L} = \{e(\mathbf{X}_i, \mathbf{X}_j, O)\}$ is the set of directed links. Each directed link $e(\mathbf{X}_i, \mathbf{X}_j, O)$ can transform the features from \mathbf{X}_i to \mathbf{X}_j using an operation O , where O is either a specific operation \mathbf{o} or a mixture operation $\bar{\mathbf{o}}$. The mixture operation $\bar{\mathbf{o}}^{(i,j)}$ is parameterized by architectural parameters $\alpha^{(i,j)}$ as a softmax mixture over all the possible operations within the operation space \mathcal{O} , *i.e.*,

$$\bar{\mathbf{o}}^{(i,j)}(\mathbf{X}_i) = \sum_{\mathbf{o} \in \mathcal{O}} \frac{\exp(\alpha_{\mathbf{o}}^{(i,j)})}{\sum_{\mathbf{o}' \in \mathcal{O}} \exp(\alpha_{\mathbf{o}'}^{(i,j)})} \mathbf{o}(\mathbf{X}_i). \quad (31)$$

For each operation $\mathbf{o}^{(i,j)}$, it is associated with the network weights $\mathbf{w}^{(i,j)}$.

The network differentiation aims to differentiate the local supernets into several specific subnets. Specifically, after network division and before network differentiation, the current architecture contains two kinds of links

$e(\mathbf{X}_i, \mathbf{X}_j, \mathbf{o})$ and $e(\mathbf{X}_i, \mathbf{X}_j, \bar{\mathbf{o}})$. After network differentiation, there is only one kind of links, *i.e.*, $e(\mathbf{X}_i, \mathbf{X}_j, \mathbf{o})$, where a valid architecture is obtained. This procedure can be implemented by some differentiable architecture search strategies (DARTS [40], SGAS [32], *etc.*). Taking DARTS as an example, the learning procedure of the architectural parameters involves a bi-level optimization problem, *i.e.*,

$$\min_{\mathcal{A}} \mathcal{L}_{val}(\mathcal{W}^*(\mathcal{A}), \mathcal{A}), \quad (32)$$

$$s.t. \mathcal{W}^*(\mathcal{A}) = \underset{\mathcal{W}}{\operatorname{argmin}} \mathcal{L}_{train}(\mathcal{W}, \mathcal{A}), \quad (33)$$

where \mathcal{L}_{train} and \mathcal{L}_{val} are the training and validation loss, respectively. \mathcal{W} is the set of network weights $\{\mathbf{w}^{(i,j)}\}$ and \mathcal{A} is the set of the architectural parameters $\{\alpha^{(i,j)}\}$. DARTS [40] proposes to solve the bi-level problem by a first/second order approximation. At the end of the search, the final architecture is derived by selecting the operation with the highest weight for each mixture operation, *i.e.*,

$$\bar{\mathbf{o}}^{(i,j)} \leftarrow \underset{\mathbf{o} \in \mathcal{O}}{\operatorname{argmax}} \alpha_{\mathbf{o}}^{(i,j)}. \quad (34)$$

C. Visualizing Hierarchical Features

In this section, we provide more examples of the learned relation and node features on ModelNet40. The visualization results are reported in Figure 7.

D. Searched Architectures

We illustrate our searched GNN architectures using the proposed *network proliferation search paradigm* in Figure 8, 9, 10, 11, 12, 13, 14, 15, 16, 17, 18, 19, 20, 21, 22, 23, 24, 25, 26.

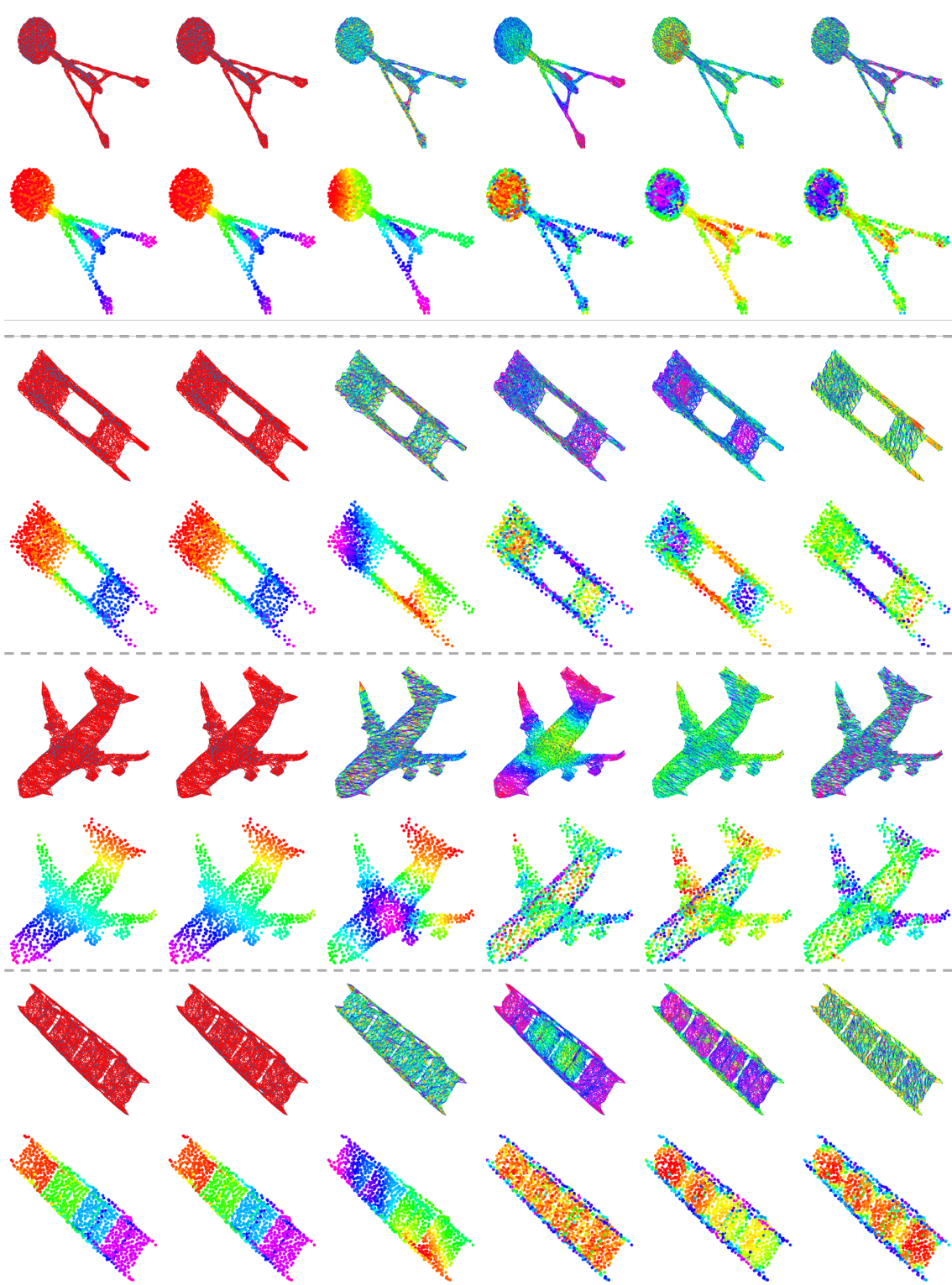


Figure 7. Visualization of the learned hierarchical relation and node features for 3D point cloud recognition. Relation features with different edge color distributions have different message-passing preferences. Node features with different node color distributions represent different clustering effects.

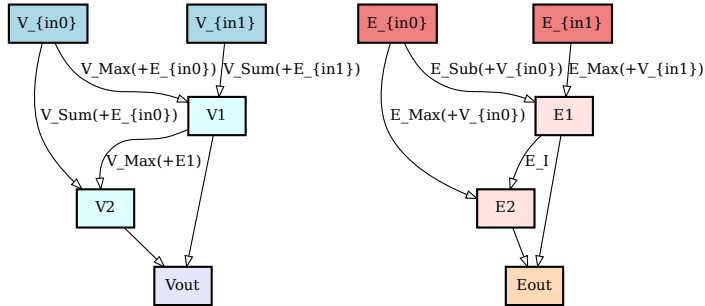


Figure 8. Illustration of the searched architecture with the size of 2 on the ZINC dataset.

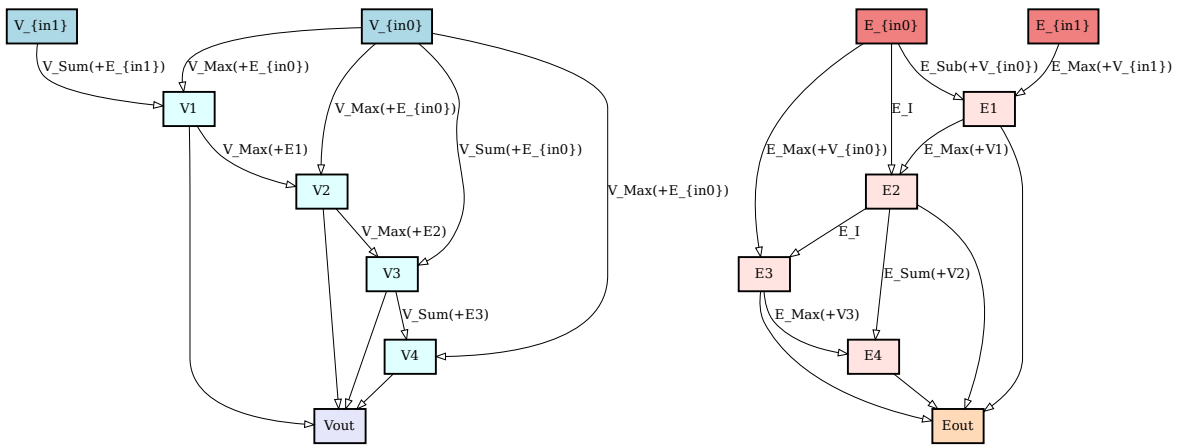


Figure 9. Illustration of the searched architecture with the size of 4 on the ZINC dataset.

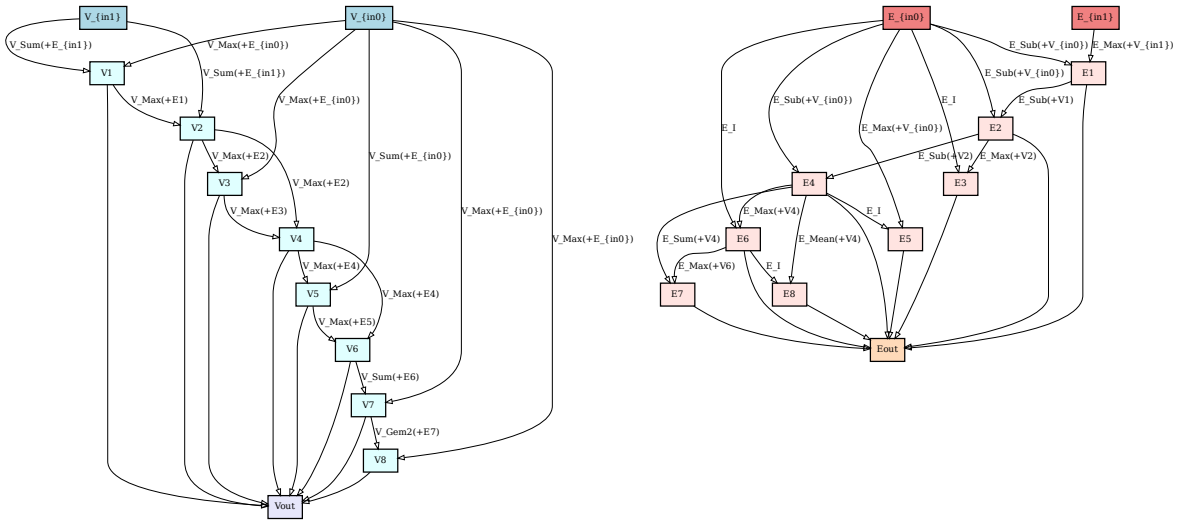


Figure 10. Illustration of the searched architecture with the size of 8 on the ZINC dataset.

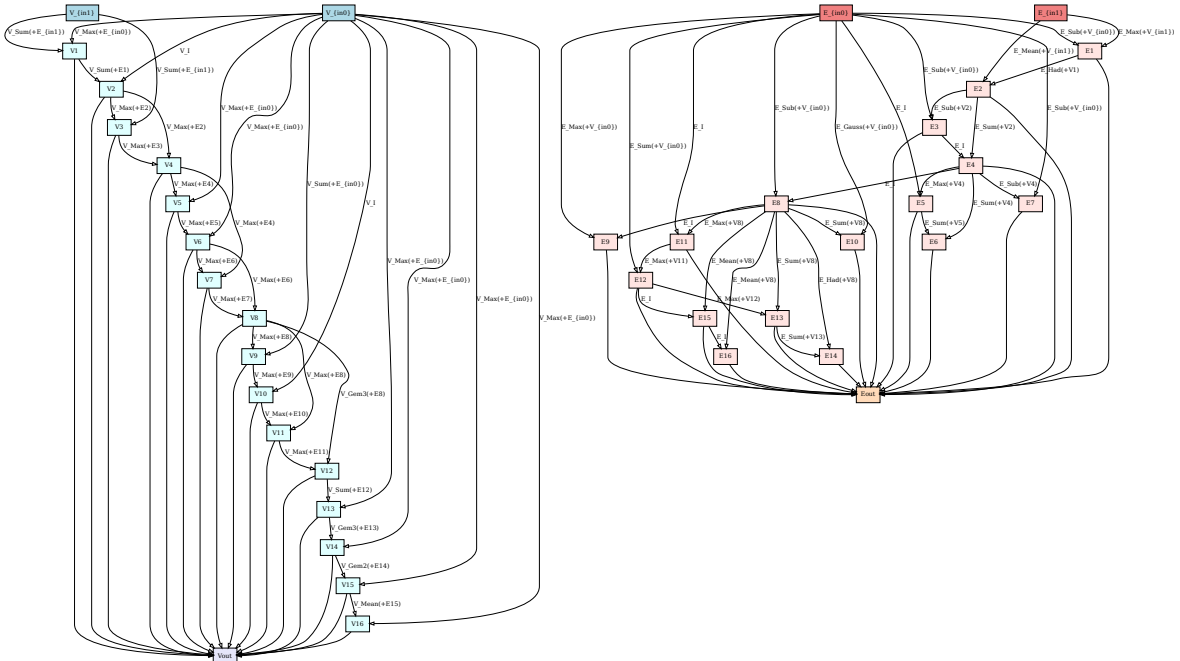


Figure 11. Illustration of the searched architecture with the size of 16 on the ZINC dataset.

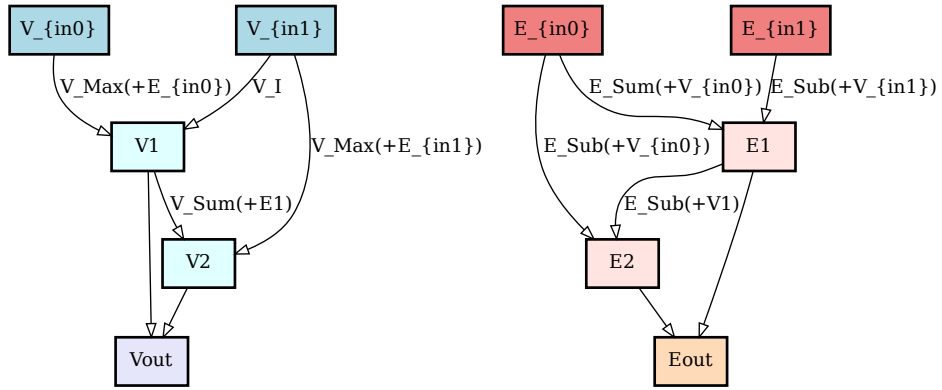


Figure 12. Illustration of the searched architecture with the size of 2 on the CLUSTER dataset.

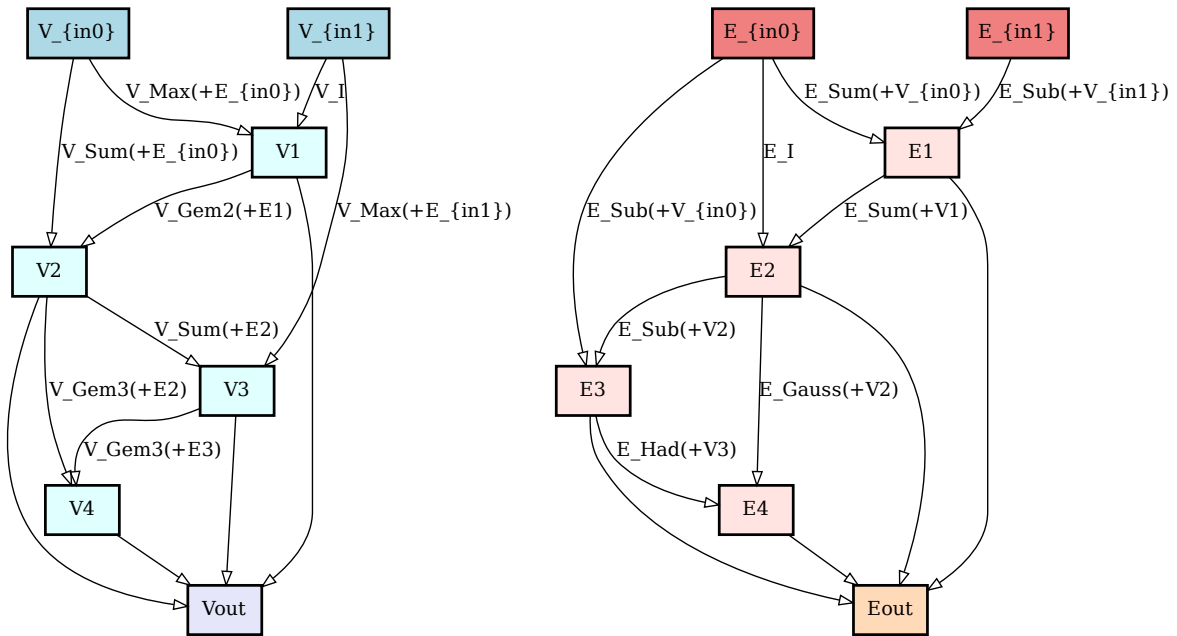


Figure 13. Illustration of the searched architecture with the size of 4 on the CLUSTER dataset.

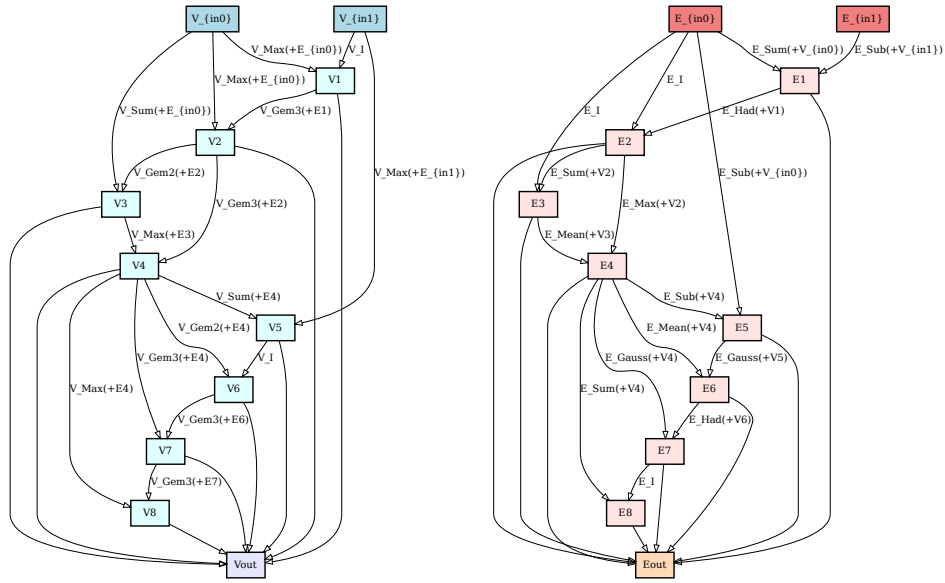


Figure 14. Illustration of the searched architecture with the size of 8 on the CLUSTER dataset.

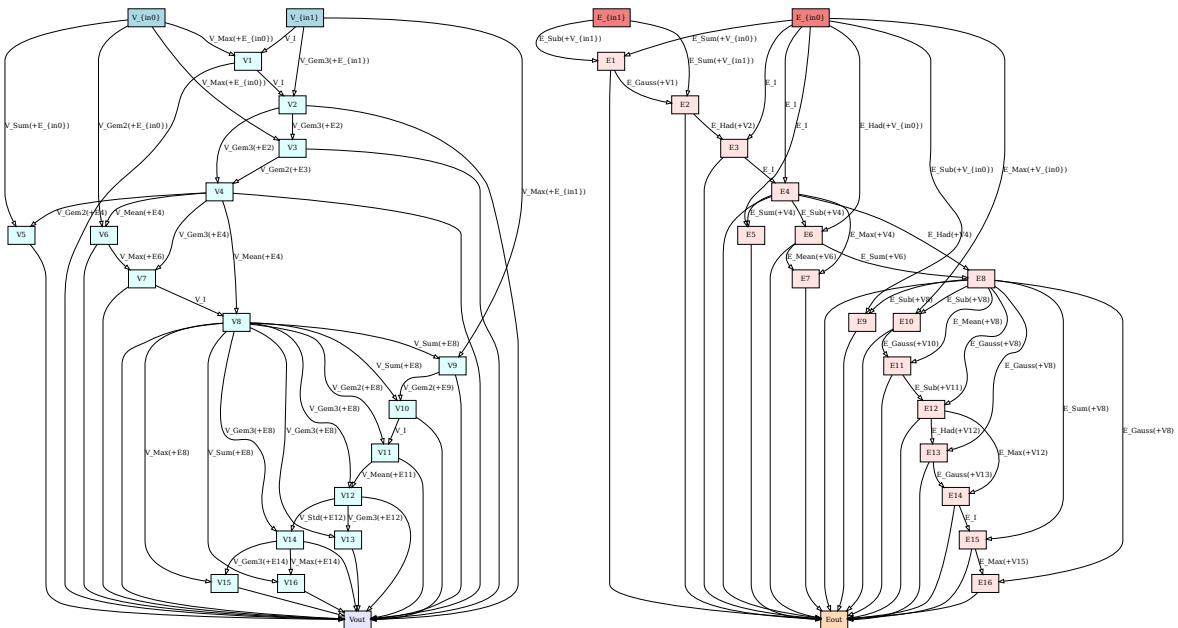


Figure 15. Illustration of the searched architecture with the size of 16 on the CLUSTER dataset.

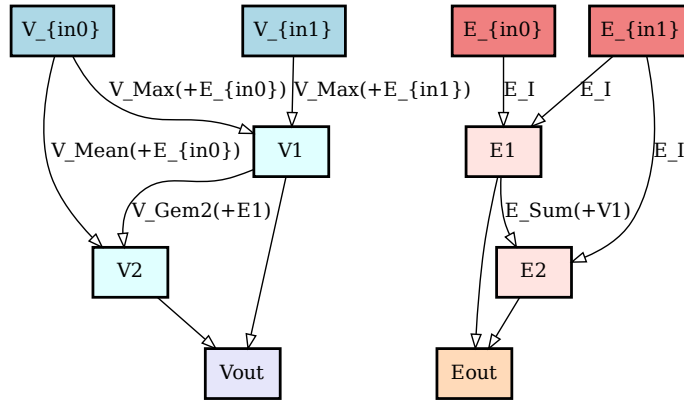


Figure 16. Illustration of the searched architecture with the size of 2 on the TSP dataset.

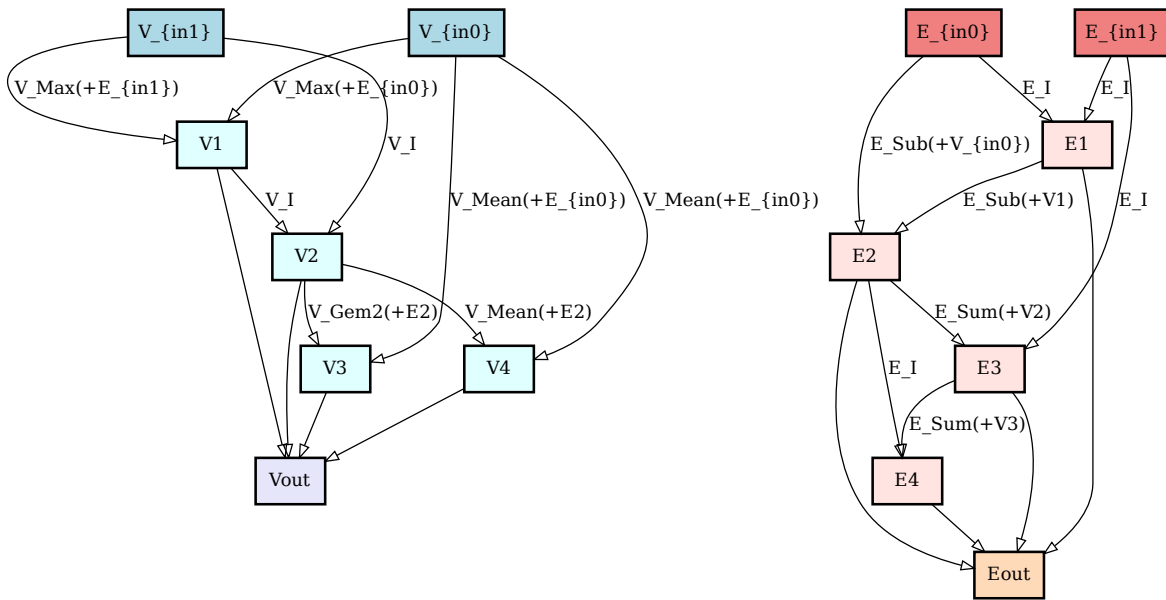


Figure 17. Illustration of the searched architecture with the size of 4 on the TSP dataset.

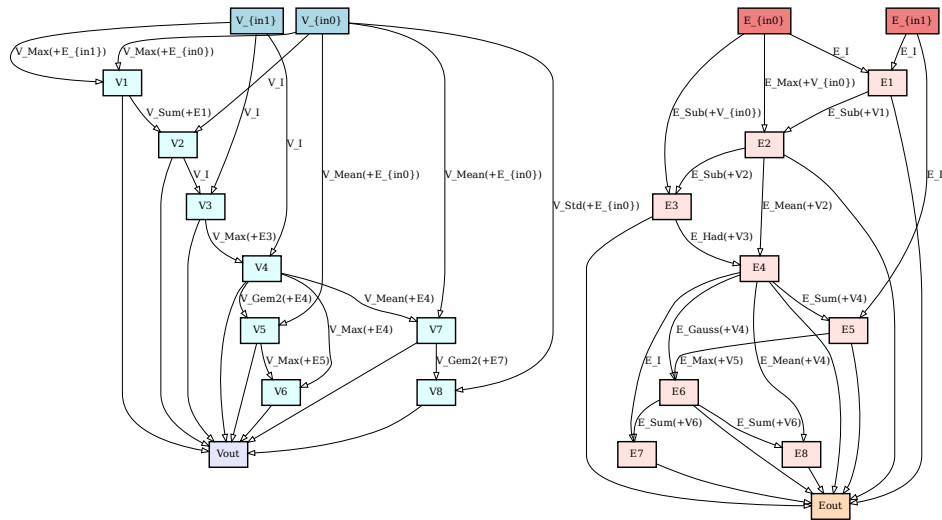


Figure 18. Illustration of the searched architecture with the size of 8 on the TSP dataset.

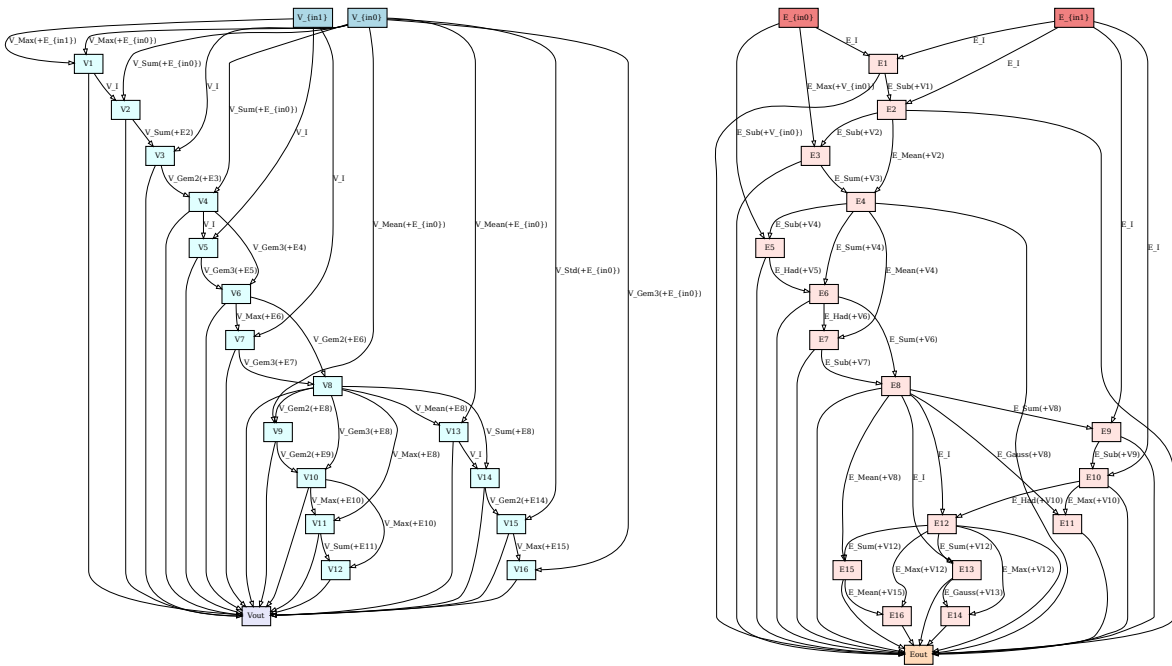


Figure 19. Illustration of the searched architecture with the size of 16 on the TSP dataset.

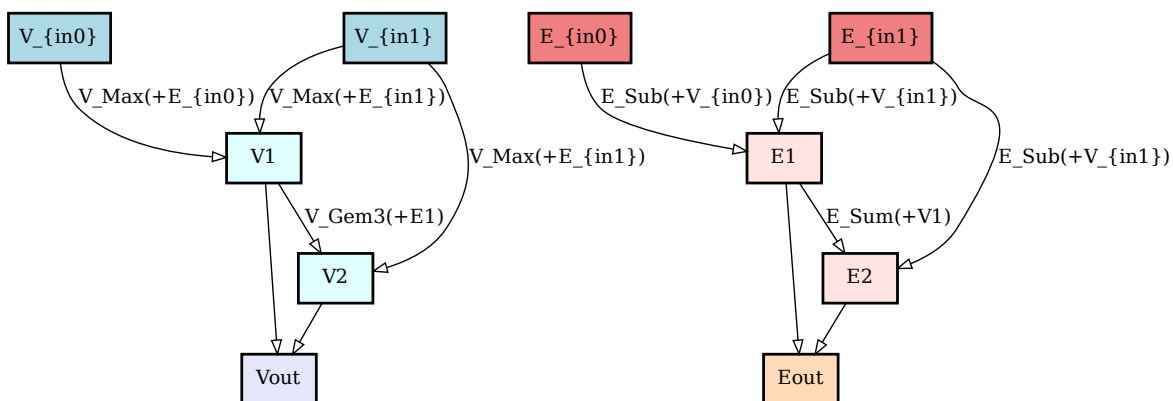


Figure 20. Illustration of the searched architecture with the size of 2 on the CIFAR10 dataset.

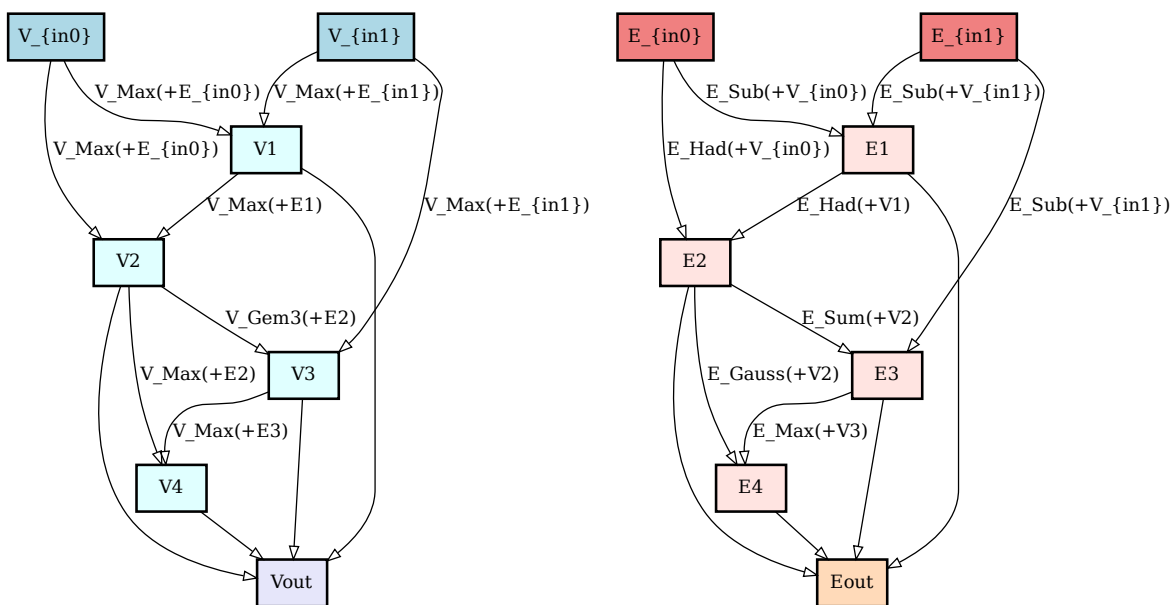


Figure 21. Illustration of the searched architecture with the size of 4 on the CIFAR10 dataset.

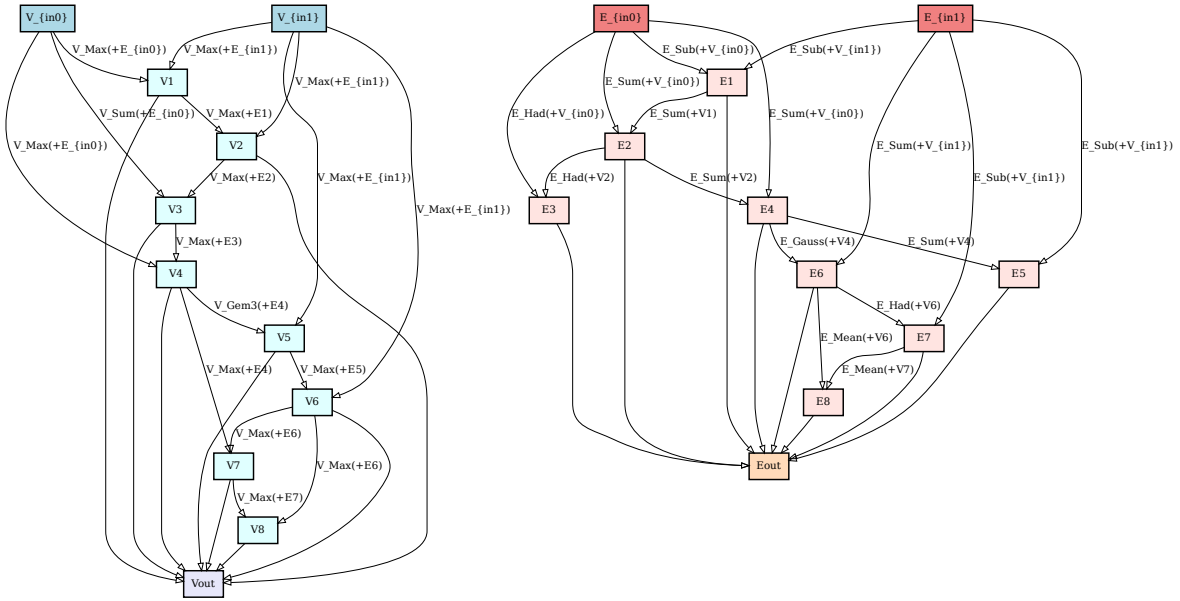


Figure 22. Illustration of the searched architecture with the size of 8 on the CIFAR10 dataset.

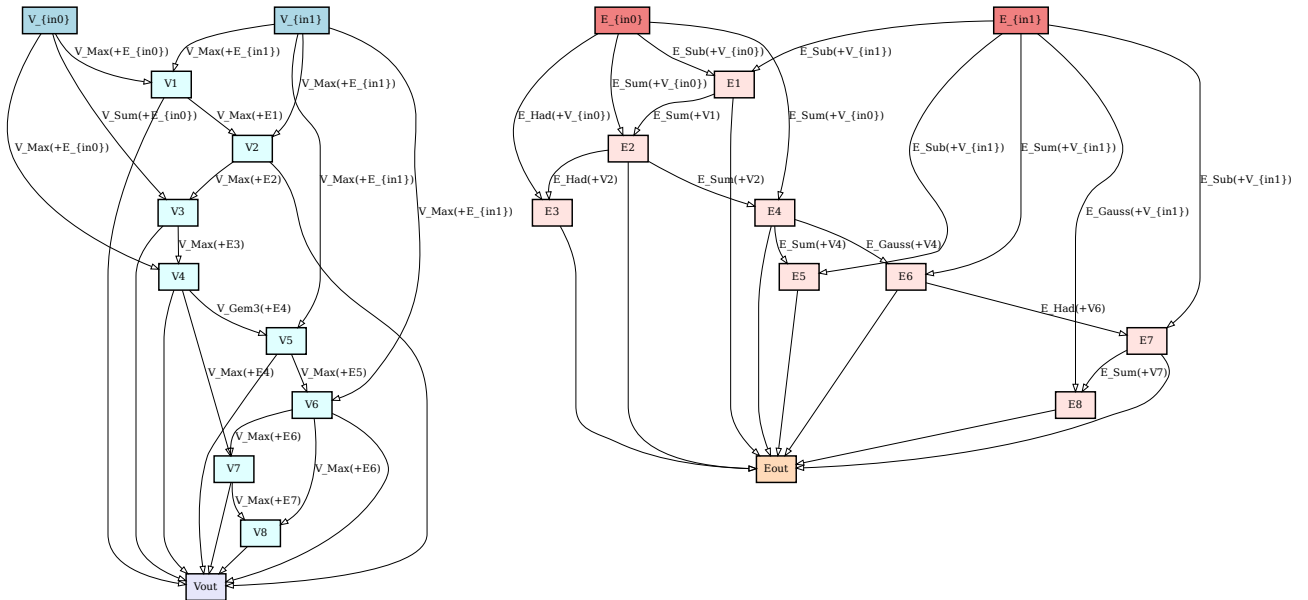


Figure 23. Illustration of the searched architecture with the size of 16 on the CIFAR10 dataset.

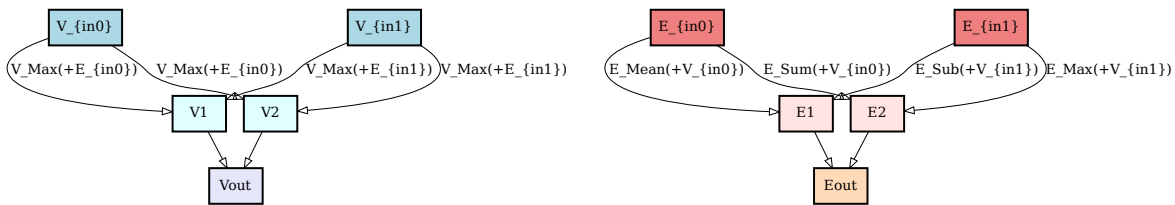


Figure 24. Illustration of the searched architecture with the size of 2 on the ModelNet10 dataset.

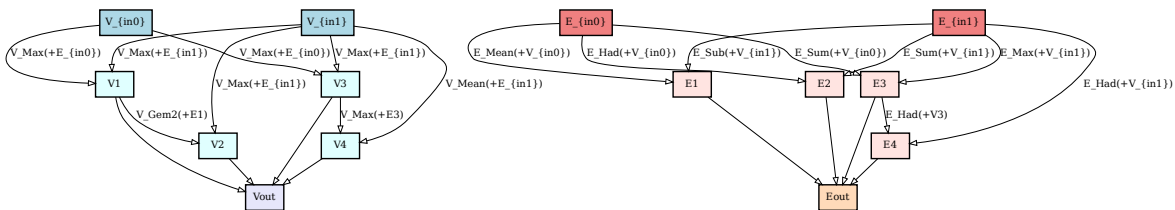


Figure 25. Illustration of the searched architecture with the size of 4 on the ModelNet10 dataset.

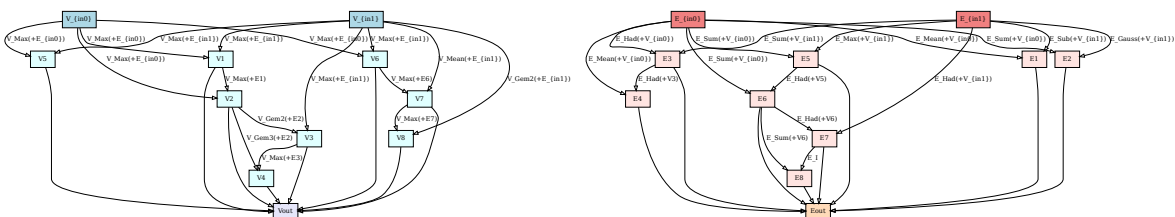


Figure 26. Illustration of the searched architecture with the size of 8 on the ModelNet10 dataset.